Research Square

Preprints are preliminary reports that have not undergone peer review.
They should not be considered conclusive, used to inform clinical practice,
or referenced by the media as validated information.

Psychotropic medications selectively reshape the human gut microbiota and alter neuroactive metabolite production

Fátima Pereira

f.c.pereira@soton.ac.uk

University of Southampton https://orcid.org/0000-0002-1288-6481

Juwairiyah Shazzad

University of Southampton https://orcid.org/0009-0003-3263-370X

Paul Afolabi

University of Southampton

William Lane

University of Southampton

Jessica Teeling

university of Southampton https://orcid.org/0000-0003-4004-7391

Jonathan Swann

University of Southampton https://orcid.org/0000-0002-6485-4529

Article

Keywords:

Posted Date: November 17th, 2026

DOI: https://doi.org/10.21203/rs.3.rs-11525173/v1

License: This work is licensed under a Creative Commons Attribution 4.0 International License.
Read Full License

Additional Declarations: There is **NO** Competing Interest.

Psychotropic medications selectively reshape the human gut microbiota and alter neuroactive metabolite production

Juwairiyah B. Shazzad[1], Paul R. Afolabi[2], William A. Lane[1], Jessica L. Teeling[1], Jonathan R. Swann[2] and Fatima C. Pereira[1]

[1]School of Biological Sciences, Faculty of Environmental and Life Sciences, University of Southampton, Southampton, UK, SO17 1BJ

[2]School of Human Development & Health, Faculty of Medicine, University of Southampton, Southampton, UK, SO16 6YD

Abstract

Psychotropic medications are widely prescribed and increasingly recognised to alter the gut microbiome. However, the mechanisms underlying these drug-microbiome interactions and their consequences for neuroactive microbial metabolism remain poorly understood. Here, we investigated the impact of commonly prescribed antidepressants and antipsychotics on gut microbiomes *ex vivo*. Among the drugs tested, sertraline and aripiprazole had the strongest effects on the gut microbiome, reducing overall microbial loads and altering the abundance of approximately 21% and 11% of microbial functional pathways, respectively. Both drugs also substantially remodelled microbial metabolism, affecting the production of microbial metabolites implicated in gut-brain signalling. Sertraline and aripiprazole both reduced indole levels, but the drugs had opposing effects on short-chain fatty acid production, which decreased with sertraline and increased with aripiprazole. Transcriptomic analyses of sertraline-exposed microbial cells revealed widespread disruption of membrane-associated transport and energy metabolism, with microscopy further supporting membrane dysfunction. By contrast, tametraline, a non-chlorinated and less lipophilic structural analogue of sertraline, produced negligible transcriptomic and microbiome-level effects. Together, our findings identify sertraline's dichlorophenyl moiety and high lipophilicity as key determinants of microbial membrane dysfunction, establishing a mechanistic link between drug chemical structure, microbiome toxicity, and metabolic remodelling.

Main

Increasing evidence indicates that the gut microbiome is closely linked to brain health and function, with several gut microbial taxa and microbial metabolites associated with improved mental health outcomes or alleviation of depressive symptoms[1-3]. These bidirectional interactions between the gut microbiome and the central nervous system are collectively described as the microbiome-gut-brain axis (MGBA)[4]. Gut microbes contribute to MGBA signalling through the production or regulation of essential neurotransmitters such as dopamine or serotonin[5,6,7]. Beyond neurotransmitters, microbial production of a wide range of neuroprotective and neuroactive metabolites represents another key mechanism through which the microbiome can shape MGBA communication[8]. These metabolites can act locally in the gut or signal to the brain by entering peripheral circulation, through activation of the vagus nerve, or by crossing the blood-brain barrier[9,10]. Among these compounds, indole and indole derivatives produced from microbial metabolism of dietary tryptophan have been implicated in host-brain signalling[11]. Indoles can modulate a range of host pathways including activation of the aryl hydrocarbon receptor which regulates host immunity both centrally and peripherally[12], and while their effects appear context-dependent, several studies have associated microbial indole production with reduced severity of depressive symptoms[12], or symptom alleviation in rats[13].

Another important class of microbial metabolites implicated in MGBA signalling are short-chain fatty acids (SCFAs), produced by gut microbes through the fermentation of complex dietary fibres[14]. SCFAs play important roles in host physiology, including maintaining gut barrier integrity[15] and regulating gut motility[16]. They are also increasingly recognised as neuroactive microbial metabolites that can influence brain function and mental health through multiple mechanisms, including modulation of neuroinflammation, blood-brain barrier integrity, neurotransmitter synthesis, and microglial maturation[17,18]. Indeed, patients with major depressive disorder had lower circulating levels of propionate and butyrate than healthy controls, and a higher baseline level of butyrate was associated with a better chance of remission[17]. Taken together, these observations imply that changes in the microbiome's ability to produce or metabolise neuroactive compounds such as indoles or SCFAs may influence MGBA signalling and mental health. Psychotropic medications that perturb these microbial functions could therefore have consequences beyond their direct effects on the central nervous system.

Consistent with this possibility, there is increasing evidence that human-targeted medications, including psychotropic drugs such as antidepressants and antipsychotics, can modulate the

human gut microbiome[19-23]. A landmark study demonstrated that several psychotropics were able to significantly inhibit the growth of commensal gut microbes in pure culture[24]. The physiological relevance of these findings is supported by evidence that antidepressant-associated alterations in the composition of the gut microbiome remained detectable in human cohorts years after the last recorded use of the medication[25]. Of note, a recent study also found that several antidepressants, including sertraline, reduced the proteome-level functional redundancy of the microbiome, with implications for microbiome resilience[26]. Despite these advances, how sertraline and other psychotropics alter the metabolic output of the human gut microbiome, and the mechanisms driving these effects, remain poorly understood. Importantly, both the efficacy and tolerability of psychotropic medications vary considerably among individuals, and this variation cannot be fully explained by genetic or environmental factors alone[27-29]. At present, it remains unclear whether drug-microbiome interactions enhance or diminish therapeutic efficacy, contribute to adverse gastrointestinal effects, or both. Therefore, it is necessary to study these interactions to enable the beneficial exploitation of the microbiome[30].

Here, we investigated the consequences of interactions between commonly prescribed psychotropic drugs and the human gut microbiome, with a particular focus on their impact on the MGBA. We supplemented gut microbiomes derived from human stool samples with physiologically relevant concentrations of six psychotropic drugs. The selected drugs *i)* reflect the most commonly prescribed antidepressants and antipsychotics in the UK[31], and *ii)* are expected to reach substantial concentrations in the colon[24]. We assessed drug-induced changes in microbial loads and community composition, and investigated their functional and metabolic consequences, including effects on microbial indole production and SCFA synthesis. We targeted these metabolites due to their high physiological luminal concentrations compared to trace neuroactive MGBA metabolites[32,33]. Finally, we identified specific structural features of sertraline that drive microbiome toxicity, establishing a mechanistic link between drug chemistry and microbiome responses.

Results

Antidepressants and antipsychotics reduce total microbial loads and alter gut microbiome composition

To assess the impact of commonly prescribed antidepressants and antipsychotics on the human gut microbiome, faecal microbial communities from six healthy donors were incubated *ex vivo*

with physiologically relevant colonic concentrations of three antidepressants (sertraline, amitriptyline and mirtazapine) and three antipsychotics (quetiapine, aripiprazole and olanzapine; Fig. 1a; Supplementary Table 1). Entacapone was included as a control due to its known detrimental effects on the gut microbiome[34]. This approach was designed to isolate the direct effects of these drugs on the microbiome while minimising confounding effects from host physiology, diet, and other factors. Total microbial cell counts revealed that sertraline consistently reduced cell counts at both 6 h and 24 h compared with the DMSO no-drug control for all donors ($P < 0.001$; Fig. 1b; Supplementary Table 2). Aripiprazole also significantly reduced total microbial abundance, but its effect was less pronounced than that of sertraline and was not observed in all individuals (Fig. 1b). In contrast, amitriptyline, mirtazapine, quetiapine, and olanzapine did not significantly alter total microbial loads relative to the no-drug control (Fig. 1b).

To understand how these drugs affect gut microbial community composition, we sequenced drug-amended samples and controls using 16S rRNA gene amplicon sequencing (Supplementary Table 3). Alpha diversity metrics did not differ significantly between drug-treated and control samples (Supplementary Fig. 1). Principal coordinate analysis based on Bray-Curtis dissimilarity followed by PERMANOVA analyses revealed significant clustering by drug treatment ($R^2 = 0.088$, $P = 0.002$) as well as by donor ($R^2 = 0.667$, $P = 0.001$) (Fig. 1c,d). The drugs contributing the most to this clustering were sertraline ($R^2 = 0.127$, $P = 0.001$) and aripiprazole ($R^2 = 0.074$, $P = 0.009$), while the remaining drugs did not contribute significantly ($P > 0.05$). Relative abundance profiles demonstrated substantial interindividual variation in baseline (t0) microbiome composition (Fig. 1e). To closely assess taxon-level responses to drug treatment, relative abundances were integrated with total cell counts to generate absolute abundance profiles (Fig. 1f). Consistent with the observed reductions in total microbial loads, sertraline and aripiprazole induced pronounced compositional shifts, whereas the remaining drugs affected comparatively few taxa (Fig. 1f). Differential abundance analysis performed using DESeq2[35] further identified significant drug-genus interactions across donors (Supplementary Fig. 2; Supplementary Table 4). Sertraline and aripiprazole affected a significant proportion of genera (23.0% ± 5.7% and 14.9% ± 7.3%, respectively). Both drugs decreased *Bacteroides*, *Collinsella*, *Fusicatenibacter*, *Parabacteroides* and *Sutterella,* while promoting the expansion of few taxa belonging to *Eubacterium* and to the Christensenellaceae family (Supplementary Fig. 2). These results identify sertraline and aripiprazole as the two drugs with the most pronounced effects on microbiome composition.

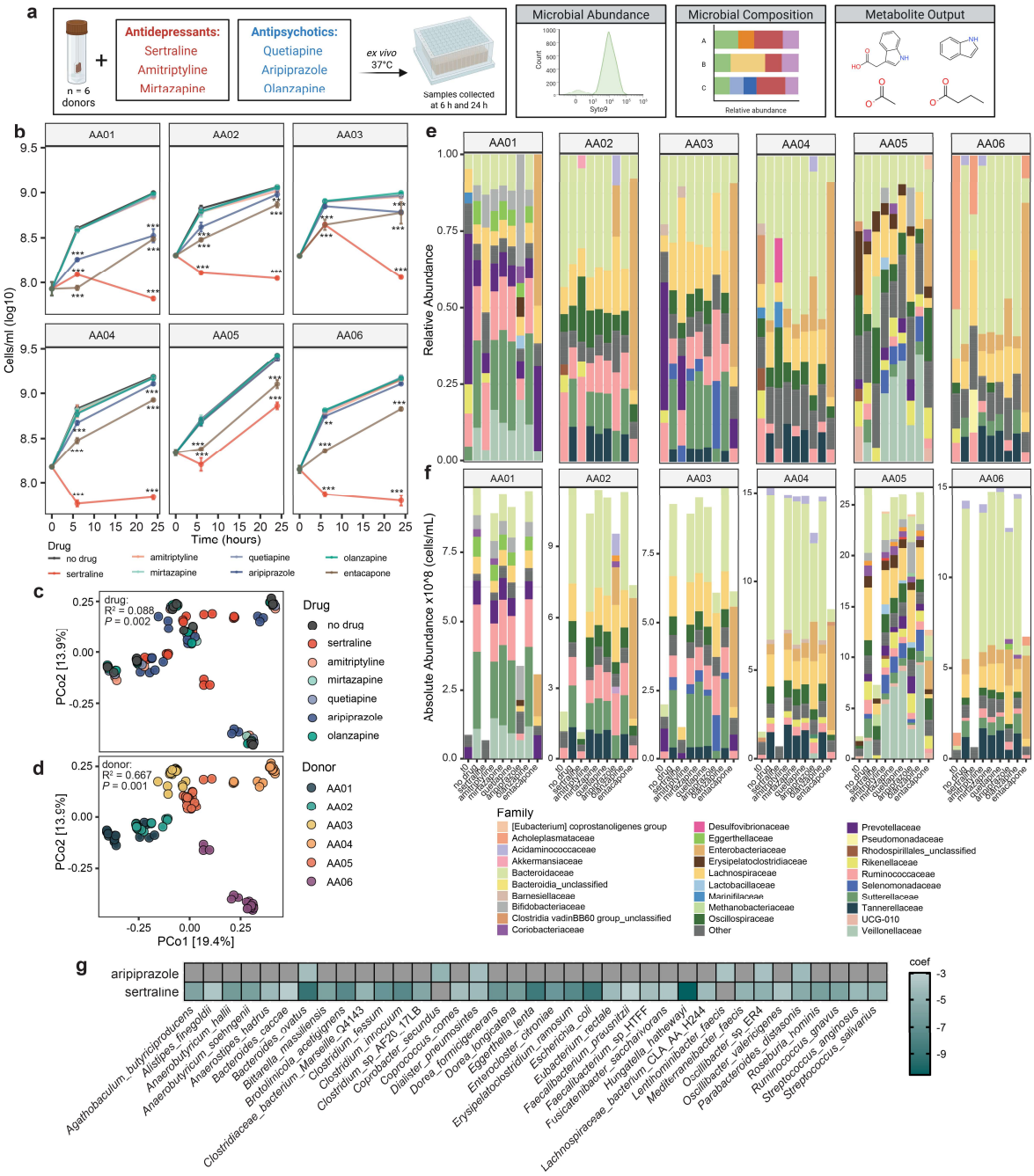


Fig. 1: Amendment of faecal samples with sertraline and aripiprazole impacted total cell counts and microbiome composition. **a**, Schematic representation of faecal sample incubations with drugs; samples were collected at the start of the incubation (t0) and after 6 and 24 h of incubation for further analyses. Created in https://BioRender.com. **b**, Total microbial cell counts across samples obtained from six donors (AA01 to AA06), as assessed by flow cytometry. Error bars represent standard deviation from mean (n = 3 technical replicates per drug per donor) and only statistically significant differences are indicated: $^{**}P < 0.01$, $^{***}P < 0.001$; ANOVA with post-hoc Dunnett's test comparing each condition to no drug at each timepoint. **c**,**d**, PCoA of microbiome samples taken at 24 h post drug amendment with (**c**) representing a comparison by drug, whereas (**d**) is a comparison by donor. Data represent 3 technical replicates per condition; n = 6. Results from PERMANOVA analyses are indicated. **e**,**f**, Relative (**e**) and absolute (**f**) family abundance profiles of faecal microbiome communities incubated for 24 h. Community composition at 0 h is also shown. All families with a relative abundance of below 0.03 or absolute abundance below 2×10^7 cells/mL were assigned to the category 'Other'. Each bar represents the mean of the triplicates. **g**, MaAsLin2 correlation heatmap of associations between drugs and absolute MetaPhlAn4 species-level taxonomic profiles of shotgun metagenomic results at 24 h post drug amendment. Coefficients > 0 indicate a positive correlation and < 0 indicate a negative correlation. Grey boxes represent no correlation. Only statistically significant associations $^{*}P < 0.05$ are displayed.

To characterise species-level responses to sertraline and aripiprazole, we performed shotgun metagenomic sequencing of drug-treated microbiomes following 24 h of incubation. Sequenced samples were analysed using MetaPhlAn[36] (Supplementary Table 5), before running a correlation analysis with MaAsLin2[37] (Fig. 1g; Supplementary Table 6). Across all donors, sertraline and

aripiprazole reduced abundances of *Bacteroides ovatus*, *Dialister pneumosintes*, *Oscillibacter* sp. ER4 and *Parabacteroides distasonis*; *Coprobacter secundus* and *Lentihominibacter faecis* were affected by aripiprazole alone, and sertraline negatively impacted an additional 29 species (Fig. 1g). Overall, the two drugs showed partially overlapping species-level effects, but sertraline affected a substantially broader range of microbial species.

Sertraline and aripiprazole alter the functional profile and resistome of the gut microbiome

To characterise drug-associated changes in microbial functional potential following sertraline and aripiprazole treatments, we profiled MetaCyc[38] microbial pathways in the shotgun metagenomic data using the HUMAnN pipeline[37] (Supplementary Table 7). Although alpha diversity of pathway profiles remained unchanged (Fig. 2a), sertraline and aripiprazole significantly altered the overall functional composition of the microbiome, as reflected by changes in pathway beta diversity (P = 0.002; Fig. 2b). Differential abundance analysis identified several pathways which were impacted significantly by sertraline and aripiprazole across all donors (21% and 11% of all identified pathways, respectively; Fig. 2c,d; Supplementary Table 8). While sertraline was predominantly associated with pathway depletion, aripiprazole was primarily linked to pathway enrichment (Fig. 2c,d). Some changes were shared between the drugs: both depleted glycan degradation pathways, potentially reflecting decreases in *Bacteroides* and other taxa with these functional capabilities (Supplementary Table 8). Both drugs also affected pathways related to SCFA production, including depletion of PWY-5677 (succinate fermentation to butanoate) following sertraline exposure. Other effects were drug-specific. Sertraline was negatively associated with multiple pathways related to the biosynthesis of menaquinol or demethylmenaquinol, the active forms of menaquinone (vitamin K2; Supplementary Fig. 3a). This may be related to the reduction in *E. coli,* a main contributor to menaquinone biosynthesis in the gut[39], observed in several donors following sertraline exposure (Supplementary Fig. 2). Several nucleotide biosynthesis and turnover pathways were also decreased (Supplementary Fig. 3a). Of the five pathways positively associated with sertraline, two were related to methanogenesis (Fig. 2c; Supplementary Table 8), consistent with an increase in the absolute abundance of *Methanobrevibacter* in three of six donors (Supplementary Figs. 2 and 3b). Aripiprazole, in contrast, was associated with an enrichment of pathways for degradation of simple sugars (glucose, sucrose, xylose) and glycogen (Fig. 2d; Supplementary Fig. 3a). Drug-specific changes were also observed for enzymes involved in indole production (Supplementary Fig. 3c).

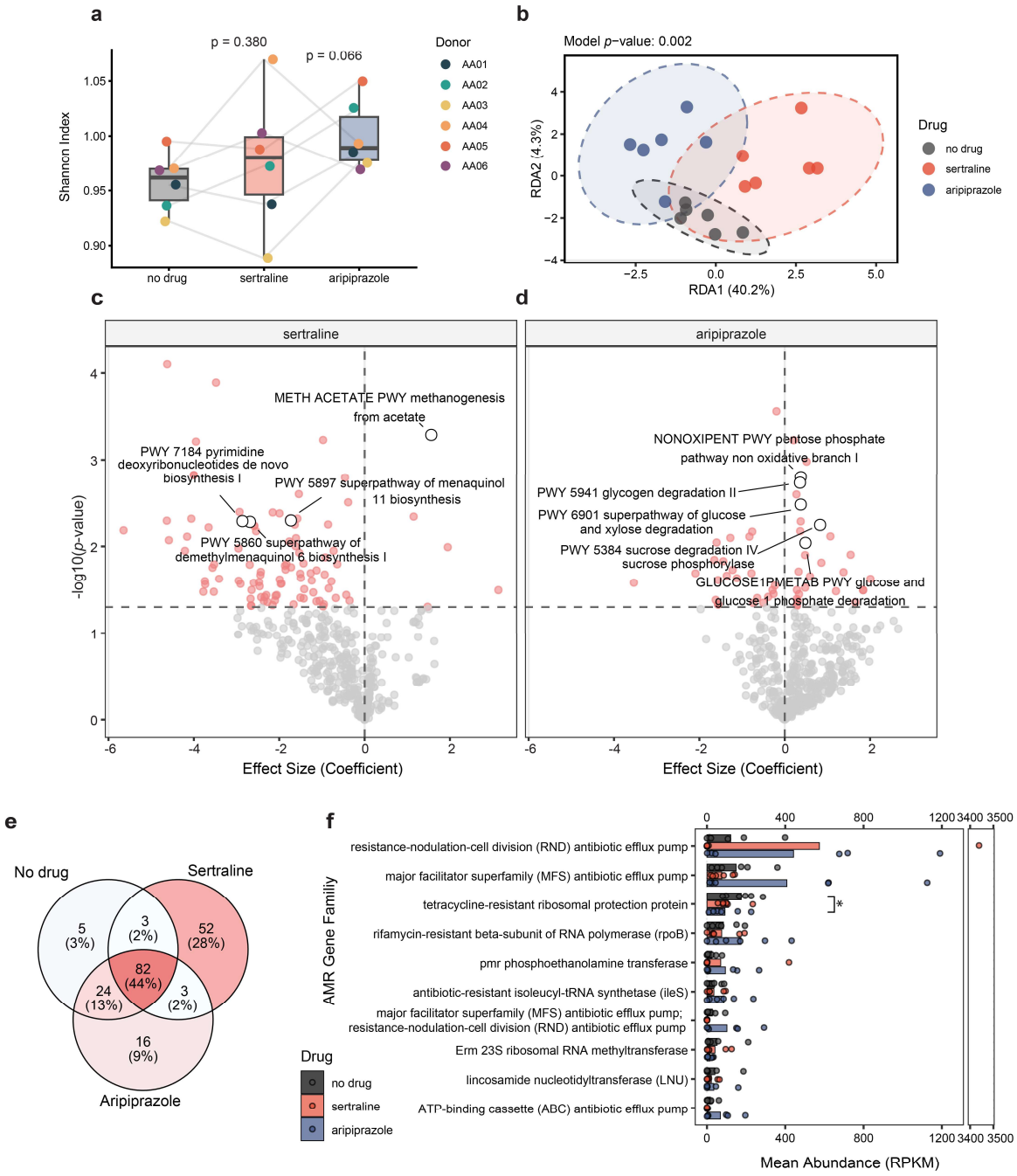


Fig. 2: Sertraline and aripiprazole altered the functional potential and resistome of the gut microbiome within 24 hours of exposure. a, Functional alpha diversity (Shannon index) of unstratified MetaCyc pathway abundances from HUMAnN 3.9. Boxes represent the median, first and third quartiles; n = 6. Whiskers extend to the highest and lowest values that are within 1.5× the interquartile range. Statistical significance was assessed using a linear mixed-effects model (LMM) with drug as a fixed effect and donor as a random effect to account for the repeated-measures design. *P*-values were calculated using Satterthwaite's method for approximating degrees of freedom (n = 6 donors, 18 total samples). **b**, Redundancy analysis (RDA) illustrating clustering of pathway profiles based on drug treatment with blocking by donor. The statistical significance of treatment effect was determined using a pseudo-F permutation test. **c**,**d**, Volcano plots of differential pathway abundances of (**c**) sertraline and (**d**) aripiprazole compared to no drug control, as assessed by MaAsLin2 with donor blocking. Statistically significant pathways $*P < 0.05$ are highlighted in red. **e**, Shared and unique antibiotic resistance ontology (ARO) terms across the different treatment conditions as assessed by RGI using the CARD database. **f,** Barplot representing the top 10 AMR gene families by drug. Mean abundance in reads per kilobase per million mapped reads (RPKM) were calculated per treatment (n = 6) with individual donor points plotted. Only significant associations $*P < 0.05$ are displayed; pairwise t-test with Benjamini-Hochberg correction.

Non-antibiotic medications have been previously linked to increased abundances of antibiotic resistance in gut bacterial isolates[40] and the microbiome[41]. We therefore profiled the gut microbiome resistome following sertraline and aripiprazole treatment, using the Resistance

Gene Identifier and CARD database[42] (Supplementary Table 9). Although most antibiotic resistance ontology (ARO) terms were shared across treatments and control, sertraline samples had more unique ARO terms (Fig. 2e), with substantial donor-specific variation (Supplementary Fig. 3c). Both drugs increased the mean abundance of ARO terms associated with resistance-nodulation-cell division (RND) efflux pumps, while major facilitator superfamily (MFS) pumps increased with aripiprazole. Conversely, tetracycline-resistance-associated ARO terms decreased significantly with aripiprazole (Fig. 2f). These results demonstrate that sertraline and aripiprazole largely increase antimicrobial resistance gene presence and abundance, with effects varying considerably between donors.

Psychotropic drugs modulate microbial indole production

We next examined whether functional changes associated with drug exposure were reflected in microbial metabolic output by quantifying indole[43], a microbial tryptophan-derived metabolite with potential neuroactive properties[13] (Supplementary Table 10). Sertraline significantly reduced indole production across all donors, consistent with the functional analyses (Fig. 3a; Supplementary Fig. 3c). Aripiprazole also reduced indole production; however, this effect was donor-dependent, with microbiomes from donors AA02 and AA06 showing no reduction compared to controls (Fig. 3a). Notably, amitriptyline also reduced indole production in three donors, despite having no significant effect on total microbial abundance or overall community composition (Fig. 3a), demonstrating that metabolic outputs can be altered independently of major compositional changes. Interindividual variability was evident, with donors AA04 and AA05 showing particularly strong reductions in indole production in response to nearly all tested drugs (Fig. 3a).

Correlation analysis identified several taxa whose abundances were significantly positively correlated with indole levels across all samples, including ASVs classified as *Bacteroides*, Lachnospiraceae spp., and *Faecalibacterium prausnitzii* (Fig. 3b), highlighting these taxa as potential contributors to microbiome-derived indole production (Supplementary Table 11). Among these, ASV_36 (*Bacteroides* unclassified) displayed a strong positive correlation with indole production and had 100% sequence identity to the type strain *B. ovatus* ATCC 8483 (Fig. 3b,c). *B. ovatus* abundance was negatively associated with sertraline and aripiprazole amendment (Fig. 1g), so to further investigate this relationship, we isolated *B. ovatus* strains from the *ex vivo* incubations. One of the isolates was a close match to ASV_36 (99.6% 16S rRNA gene similarity) and to *B. ovatus* ATCC 8483 (99.74% similarity). Both the type strain and the isolate produced substantial levels of indole from tryptophan and showed concentration-dependent

growth inhibition by sertraline and aripiprazole (Fig. 3d,e). Together, these findings demonstrate that select psychotropics suppress microbial indole production, at least partly through inhibition of indole-producing taxa such as *B. ovatus*, with potential implications for gut homeostasis and microbiome-mediated gut-brain signalling.

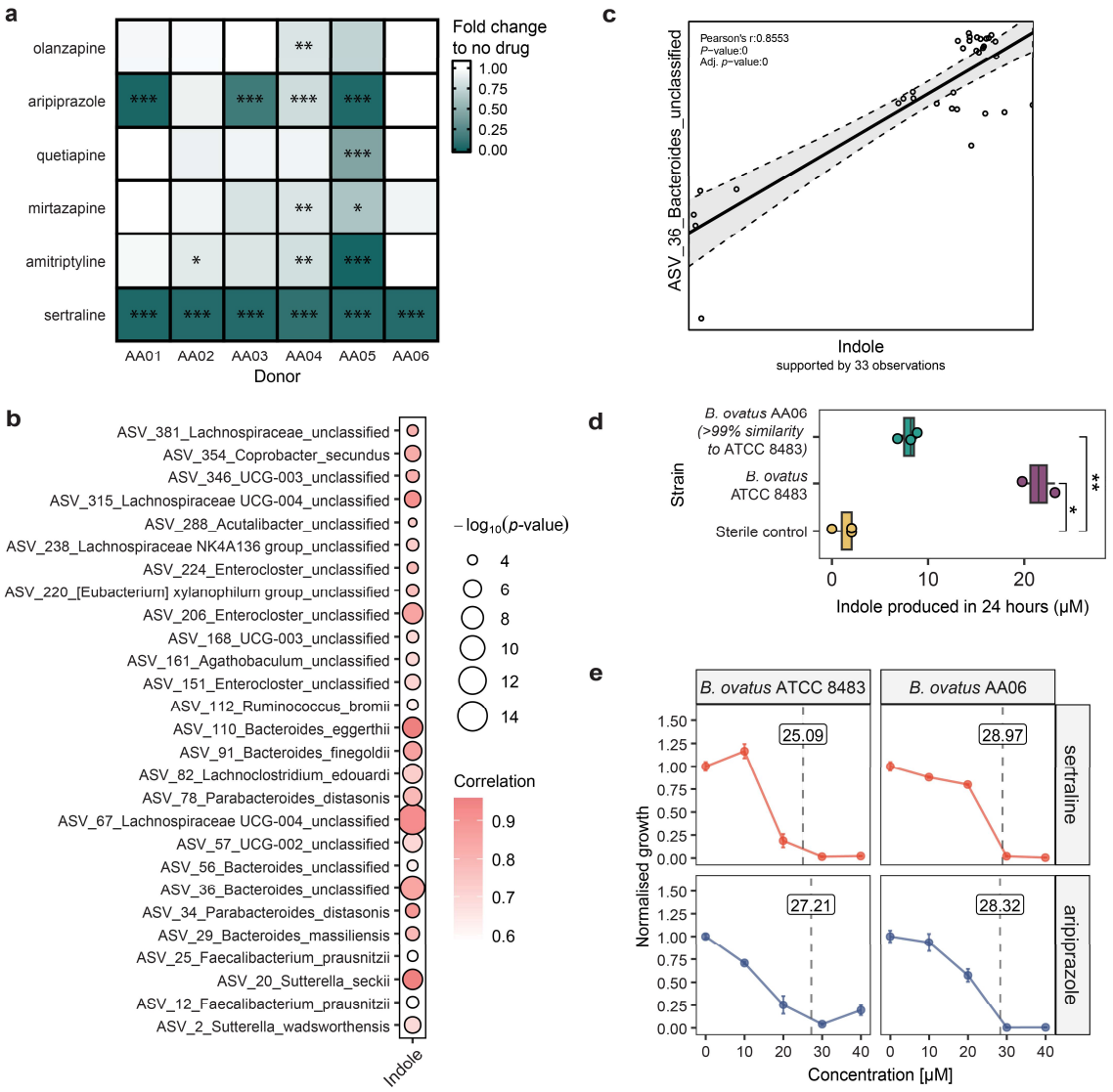


Fig. 3: Psychotropic-induced shifts in microbial taxa are associated with an overall decrease in neuroactive indole production. **a**, Heatmap indicating the fold change to no drug in indole concentrations of incubation supernatants at 24 h post drug amendment. *P*-values were calculated using one-way ANOVA with post-hoc Dunnett's test using 'no drug' as reference. **b**, Pearson's correlation between 16S rRNA gene amplicon sequencing results and indole concentrations using the Rhea pipeline. Only significant correlations with ****Padj* < 0.001 are displayed. **c**, Scatter plot of the significant positive correlation between ASV_36_Bacteroides_unclassified (which is highly identical to *Bacteroides ovatus*) and indole. **d**, Box plot showing indole produced in 24 h in supernatants of *B. ovatus* ATCC 8483 and a *B. ovatus* isolate from AA06 cultured in tryptophan-rich mGAM medium. Data represent the mean ± standard deviation. *P*-values were calculated using pairwise two-sample *t*-tests comparing each bacterial strain back to the sterile control. **e**, Normalised growth of *B. ovatus* ATCC 8483 and a *B. ovatus* isolate from AA06 following treatment with increasing concentrations of sertraline and aripiprazole. Growth was normalised to the untreated control. Data points represent the mean ± standard error of the mean across biological replicates (n = 3). Solid lines directly connect mean growth values across concentrations. Vertical dashed lines and boxed numerical callouts indicate the interpolated IC_{90} values (concentration resulting in 90% growth reduction relative to control). In **a** and **d**, only statistically significant differences are indicated with asterisks: *$P < 0.05$, **$P < 0.01$, ***$P < 0.001$.

Psychotropic drugs influence response to dietary fibres and short-chain fatty acid production

Given the importance of SCFA production in mental health[17], we next investigated whether psychotropic drugs affect microbial response to key dietary fibres and subsequent SCFA production. Donor-derived microbiomes were incubated with two fibre mixes as the sole carbon and energy source (FM1: corn, arabinoxylan, betaglucan; FM2: pectin, inulin, raffinose). Microbiome responses were assessed using bioorthogonal non-canonical amino acid tagging (BONCAT)[44] to identify translationally active microbial cells. In the absence of drugs, 42.7% and 32.7% of microbial cells responded to FM1 and FM2, respectively, compared with ~4.2% without fibre supplementation (Supplementary Fig. 4). Sertraline-treated samples consistently displayed very low fluorescence signals (2.2%) in response to both FM1 and FM2 across all donors, compared to controls (Supplementary Fig. 4; Supplementary Table 12). Indeed, sertraline exhibited a clear and consistent shift away, in terms of quantified activity fractions, from no-drug controls (Fig. 4a,b; delta fold changes). In contrast, the other drugs did not show a consistent inhibitory effect, with donor-specific responses observed (Fig. 4a,b). For most donor-drug combinations, responses to both fibre mixes tended to be affected in the same direction (Fig. 4a,b).

To further identify which members of the microbiome responded to fibre supplementation, and how drug supplementation shifts responsive populations, active fractions (BONCAT-positive cells) were sorted by fluorescence-activated cell sorting and subjected to 16S rRNA gene amplicon sequencing (Supplementary Table 3). Only samples exhibiting significant shifts in either direction relative to no drug controls ($P < 0.01$) were sorted, and sertraline was excluded due to a lack of detectable microbial activity. Active fractions were dominated by saccharolytic genera such as *Blautia*, *Faecalibacterium, Anaerostipes* or *Bifidobacterium* (Fig. 4c). Differential abundance analysis revealed that aripiprazole produced the largest number of changes across donors. This included decreases in genera such as *Mediterraneibacter* and *Paenibacillus* in response to FM1, and a decrease in *Faecalibacterium* in response to FM2, accompanied by increases in *Bifidobacterium* and *Blautia* (Fig. 4d). While aripiprazole significantly altered the taxonomic composition of active microbial populations in the presence of fibre, this was not observed across all sorted samples, despite significant shifts in activity (Fig. 4a,b,d). This suggests that drug-driven changes in fibre response reflect both changes in microbial translational activity within individual taxa and shifts in the taxa contributing to that activity.

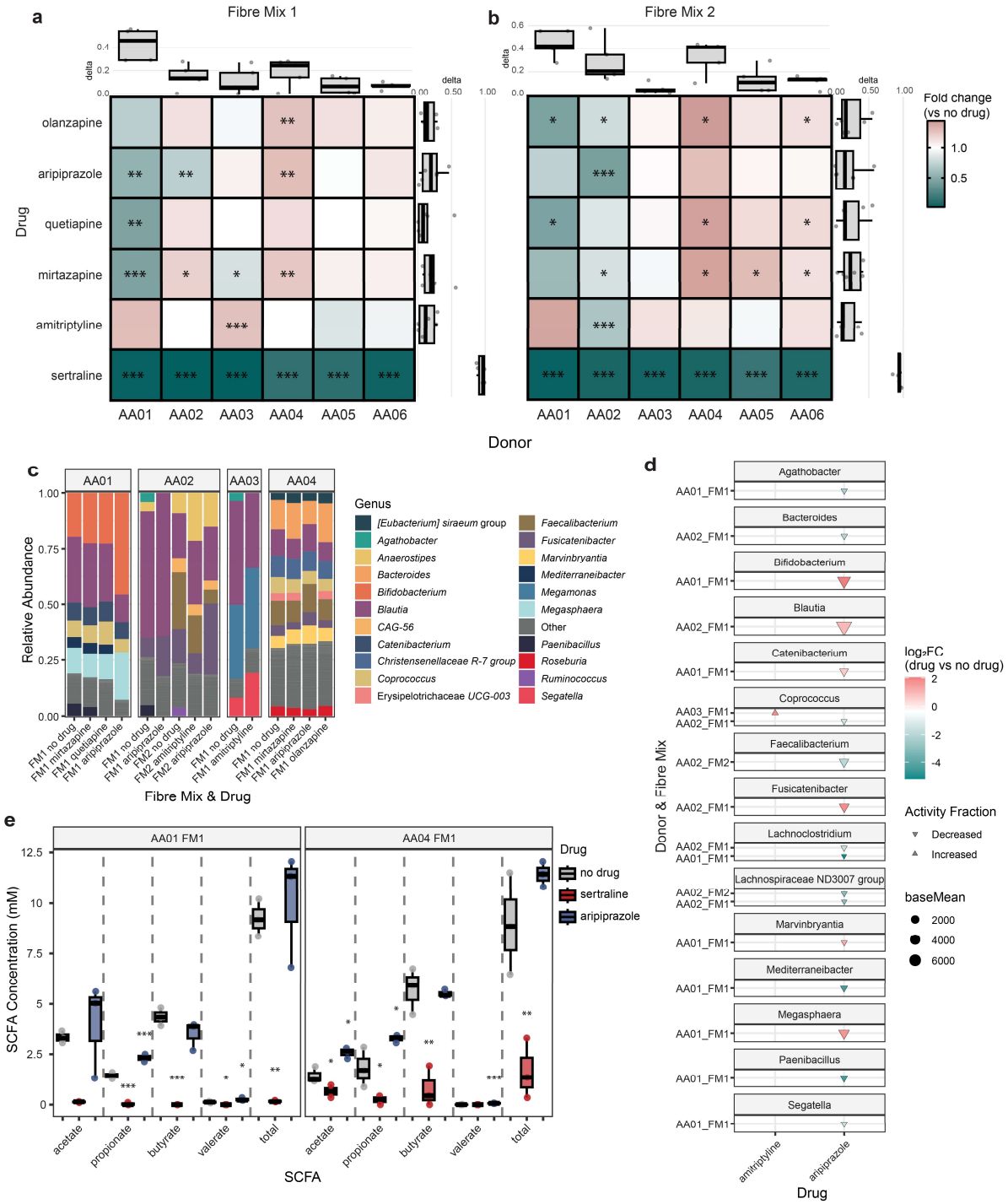


Fig. 4: Exposure to psychotropics reshaped microbiome community structure in fibre-rich environments and impacted its dietary fibre-degrading capacity. a,b, Heatmap of activity fractions assessed by BONCAT in samples supplemented with (**a**) fibre mix 1 and (**b**) fibre mix 2 for 6 h. Data are represented as a fold change to no drug; n = 6 with 3 biological replicates per condition. The magnitude of the difference across donors is also indicated as a delta fold change. **c**, Barplot of the community composition of BONCAT-positive fractions at genus level as assessed by 16S rRNA gene amplicon sequencing following 24 h supplementation with fibre mixes. All genera with a relative abundance of below 0.03 were assigned to the category 'Other'. Bars represent mean of replicates. **d**, Bubble plot from DESeq2 results of BONCAT-positive samples sorted with FACS. Data represent log2 fold change compared to no drug samples of each respective donor and only significant *$Padj$ < 0.05 are displayed. **e**, SCFA concentrations (quantified by GC-MS) in the supernatants of selected samples supplemented with fibre mix 1 and amended with drug for 24 h. Boxes represent the median, first and third quartiles. In **a** and **b**, only statistically significant differences are indicated with asterisks: *P < 0.05, **P < 0.01, ***P < 0.001; one-way ANOVA with post-hoc Dunnett's test using no drug as reference. In **e**, only differences with a significant *$Padj$ are indicated; pairwise t-test with Benjamini-Hochberg correction. FM1 = Fibre mix 1; FM2 = Fibre mix 2.

SCFAs were subsequently quantified in incubation supernatants (Supplementary Table 13). We focused on donors that had the biggest shifts in microbial activity in response to FM1, since this

fibre mix had higher activity fractions compared to FM2 overall (Supplementary Fig 4). Substantial levels of SCFAs were detected in no-drug samples (~10 mM total SCFAs; Fig. 4e). However, levels of both total and individual SCFAs plummeted for sertraline-treated samples, consistent with the extremely low activity levels detected in these samples (Fig. 4a,e). In contrast, aripiprazole treatment was associated with significantly increased levels of propionate and valerate, as well as an increasing trend for acetate (Fig. 4e). This can be explained by a shift in fibre-responsive populations (Fig. 4d), and/or an increase in SCFA production per active cell. Overall, these results suggest that sertraline completely inhibits microbial response to dietary fibres and significantly decreases SCFA output. The remaining drugs had milder effects, in some cases leading to increased activity in response to fibre, which for aripiprazole translated into donor-specific increases in SCFA levels.

Chlorination of sertraline as a driver of microbiome toxicity

Out of the six-drug panel investigated here, sertraline consistently had pronounced effects on microbiome composition and metabolic output, prompting further investigation into the structural basis of these effects. Sertraline contains a dichlorophenyl group (Fig. 5a), and halogenated aromatic compounds, including those with chloro substituents, can resist microbial degradation and accumulate in microbial cells, leading to toxicity[45]. To investigate whether this structural feature contributed to the effects of sertraline on the microbiome, we tested tametraline, a sertraline analogue lacking the dichloro moiety[46]. Although tametraline did cause a slight reduction in total microbial abundance across all donors, this effect was negligible compared with that of sertraline (Fig. 5b; Supplementary Table 14). Consistent with this observation, 16S rRNA gene amplicon sequencing revealed that tametraline-treated communities closely resembled no-drug controls, whereas sertraline-treated communities formed a distinct cluster (Fig. 5c; Supplementary Table 15). Similarly, tametraline had no significant effect on indole production (*Padj* > 0.05; ANOVA with post hoc Dunnett's test; Supplementary Table 16).

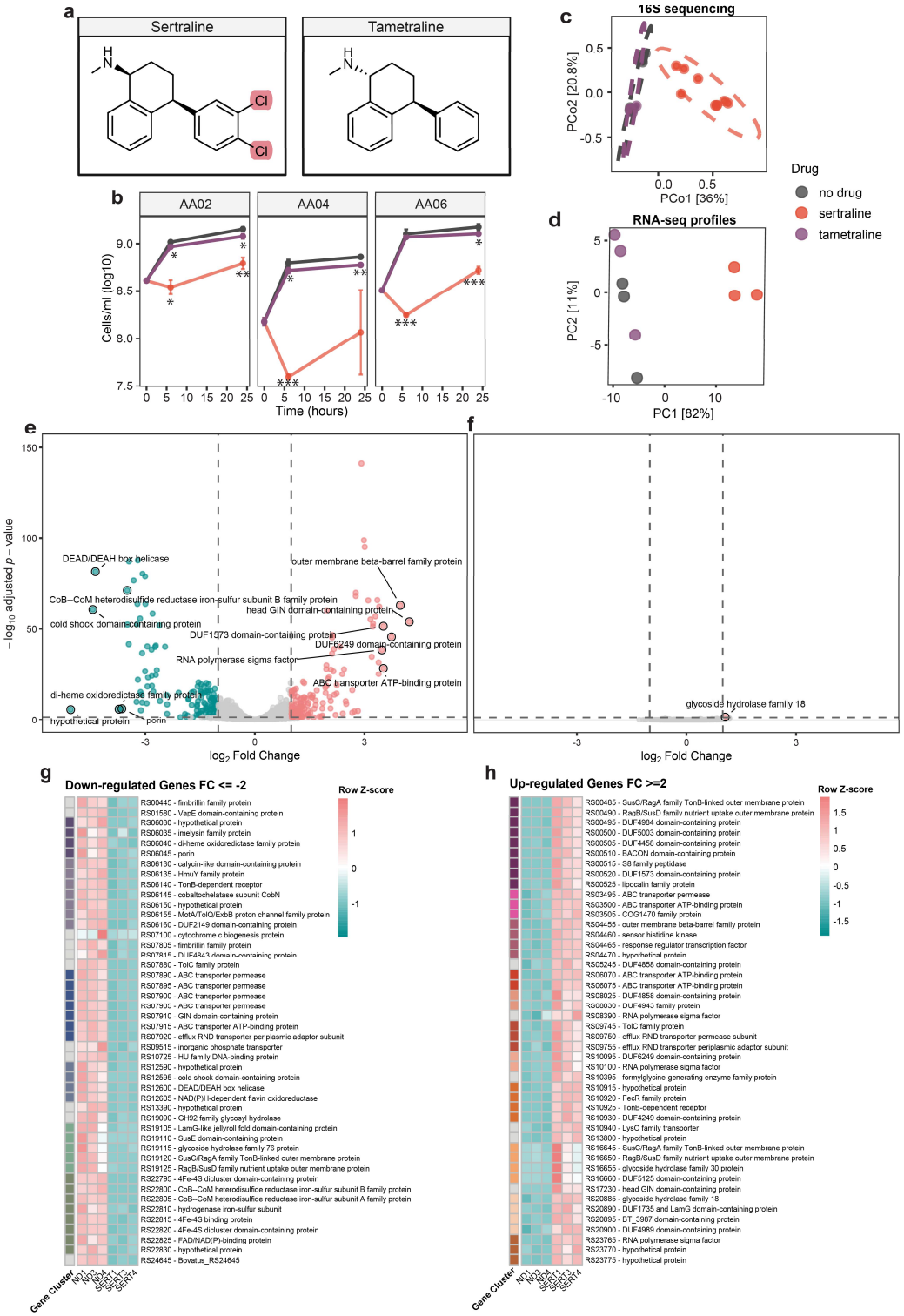


Fig. 5: Multiple halogenation of sertraline contributes to its toxicity towards the microbiome and alters gene expression of *Bacteroides ovatus*. a, Chemical structures of sertraline and tametraline. **b**, Total microbial cell counts of AA02, AA04 and AA06 expressed as log10 (cells/mL) over the incubation period, as assessed by flow cytometry. Samples were taken at the start of the incubation (t0) and after 6 and 24 h of incubation. Error bars represent standard deviation from mean (n = 3 technical replicates) and only statistically significant differences are indicated: **P* < 0.05, ***P* < 0.01, ****P* < 0.001; ANOVA with post-hoc Dunnett's test comparing each condition to no drug at each timepoint. **c**, PCoA of 16S rRNA gene amplicon sequencing profiles at 24 h post drug amendment. **d**, PCA of rlog-transformed RNA-seq read counts from *B. ovatus* cultures grown in a DMSO no-drug control, sub-inhibitory sertraline, and tametraline. Samples were collected at mid-exponential phase. **e**,**f**, Volcano plot of DEGs of *B. ovatus* when exposed to (**e**) sertraline and (**f**) tametraline. **g**,**h**, Heatmap of all significantly (**g**) downregulated and (**h**) upregulated genes of *B. ovatus* when exposed to sertraline. Only DEGs which have a fold change of >= 2 or <= 2 and a **Padj* < 0.05 are included.

To investigate the molecular basis of the effect of sertraline on the microbiome, we performed transcriptomic analyses of *B. ovatus* ATCC 8483, a taxon strongly affected by sertraline, when

grown at sub-inhibitory concentrations of either sertraline or tametraline (see methods; Supplementary Fig. 5a). Principal component analysis of the resulting transcriptomic profiles revealed that sertraline-treated samples clustered separately from both tametraline-treated samples and the no-drug control (Fig. 5d). Differential expression analyses identified 271 differentially expressed genes (DEGs) in sertraline samples, accounting for 5.5% of the genome. In contrast, only a single DEG was observed following tametraline treatment (Fig. 5e,f; Supplementary Table 17). Sertraline-responsive genes showed highly concordant changes relative to both no-drug control and tametraline treatment (Spearman's $\rho = 0.967$; Supplementary Fig. 5b).

Among sertraline DEGs, a DEAD/DEAH box helicase with established roles in RNA remodelling and ribosome biogenesis[47], and a cold shock domain-containing protein which functions as an RNA chaperone[48], were among the most strongly downregulated genes (Fig. 5e). These proteins were located within a cluster of four consecutive downregulated genes (Fig. 5g), suggesting altered RNA metabolism and translational capacity, consistent with the reduced growth observed in sertraline-treated cultures. Importantly, the transcriptional response was dominated by the enrichment of membrane-associated genes among sertraline-induced DEGs. PSORTb[49] predictions revealed that 59% of DEGs encoded cell envelope- or membrane-associated proteins, compared to only 36% of the baseline *B. ovatus* proteome (Supplementary Fig. 5c; Odds ratio = 2.55, $P = 1.17 \times 10^{-8}$, Fisher's exact test), supporting a membrane-targeted mode of action. *Bacteroides* spp. are well known for their ability to degrade complex polysaccharides[50], and several membrane-associated DEGs involved in polysaccharide sensing, binding, and transport were identified, including genes encoding SusC/RagA and RagB/SusD outer membrane family proteins (Fig. 5g,h). In addition, several gene clusters associated with cellular energetics were significantly downregulated. These included genes encoding multiple 4Fe-4S-containing proteins, a hydrogenase iron-sulfur subunit and CoB-CoM heterodisulfide reductase family proteins (Fig. 5g), pointing to a coordinated disruption of membrane-associated electron transfer and cellular energetics. These redox-associated transcriptional shifts occurred alongside extensive differential expression of key membrane transport systems, including TonB-dependent receptors, ABC transporters, the SusC/SusD proteins, and RND efflux transporters (Fig. 5g,h). Together, these findings indicate substantial remodelling of cell envelope-associated transport and metabolic functions.

To assess whether sertraline causes gross cell envelope or morphological defects, we imaged *B. ovatus* cells by scanning electron microscopy (Fig. 6a). Sertraline-treated cells showed a loss of

their characteristic rod-shaped rigidity, with several cells appearing concave, and a subset were severely elongated (Fig. 6a; white and yellow arrows, respectively). These phenotypes were specific to sertraline: tametraline-treated cells resembled the untreated control (Fig. 6a). Additionally, sertraline treatment significantly increased membrane permeability, with elongated cells exhibiting particularly strong propidium iodide staining, indicative of compromised membrane integrity (Fig. 6b,c). One explanation is the higher lipophilicity of sertraline (partition coefficient = 4.8) compared to tametraline (partition coefficient = 3.5)[51], which is largely attributable to its dichloro moiety[52]. These findings support a model in which the dichlorophenyl group promotes sertraline partitioning into the bacterial cell envelope, disrupting membrane integrity and associated transport and energy-transducing processes, with downstream effects on cell morphology and growth (Fig. 6d).

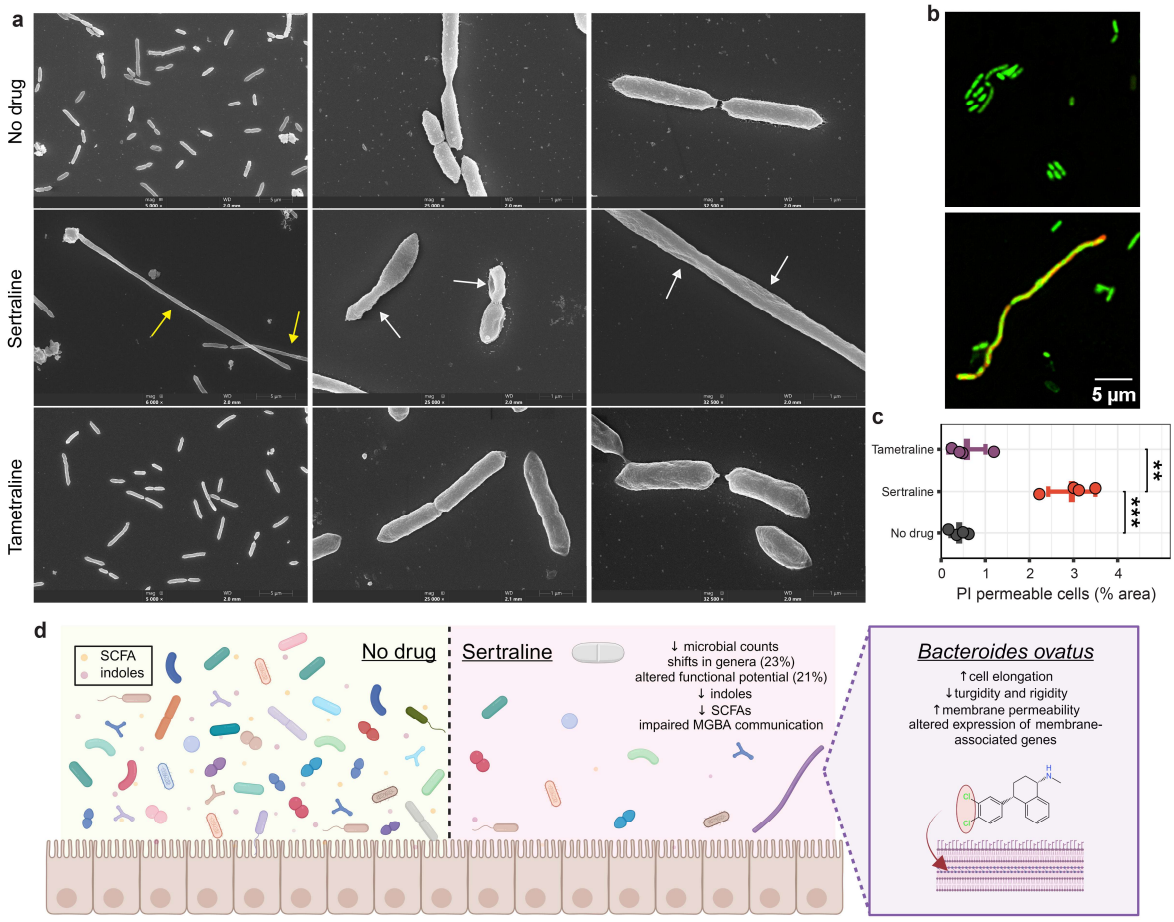


Fig. 6: Multiple halogenation of sertraline alters cell morphology and permeability of *Bacteroides ovatus*. **a**, Scanning electron microscopy micrographs of *B. ovatus* cells treated with DMSO control, 30 µM sertraline, or 30 µM tametraline. Yellow arrows indicate filamentation, whereas white arrows point to defects in cell structure or turgidity. The magnification (mag), working distance (WD) and scale bar is stated below each image. **b**, Representative fluorescent images of *B. ovatus* in the no drug control (top) and sertraline-treated (bottom) conditions, stained with Syto9 (green, live/all cells) and propidium iodide (red, membrane-compromised/dead cells). Scale bar is indicated in the sertraline-treated image. **c**, Propidium iodide (PI)-stained area as a percentage of Syto9-stained area after treatment with DMSO, sertraline and tametraline. Points show technical replicates (n = 4 per group) and bars show mean ± SD. Data were log10-transformed and compared by one-way ANOVA followed by Tukey's HSD test; only significant differences are shown. $^{**}P < 0.01$, $^{***}P < 0.001$. **d**, Schematic representation of sertraline's effect on the human gut microbiome and on *B. ovatus*. SCFA = short-chain fatty acid; MGBA = microbiome-gut-brain axis. Created in https://BioRender.com.

Discussion

As psychotropic medication use rises globally[31], understanding how these drugs interact with the gut microbiome is increasingly important, given their potential to influence treatment efficacy and tolerability[53]. Here, we demonstrated that commonly prescribed antidepressants and antipsychotics can impact gut microbial communities on multiple levels. Exposure to sertraline and aripiprazole reduced total microbial loads, with communities amended with sertraline unable to recover within 24 hours (Fig. 1b). In addition to shifts in microbial loads, both sertraline and aripiprazole significantly altered the functional potential of the donor microbiomes, particularly of pathways involved in simple sugar metabolism and nucleotide and vitamin biosynthesis. Sertraline significantly depleted the pathways linked to menaquinol (vitamin K2) biosynthesis (*E. coli*). This finding is consistent with previous studies that have identified *E. coli* as a key producer of this vitamin[39]. Remarkably, vitamin K2 supplementation significantly improved depression status in women[54], suggesting that restoring this sertraline-disrupted pathway could potentially improve therapeutic outcomes.

We next investigated the impact of these drugs on the gut microbiome at the metabolite level. Indoles have previously been associated with neurogenesis, neuroprotection, and antidepressant-like activity, highlighting their potential importance in MGBA signalling[13,55,56]. In the present study, all tested drugs reduced microbial indole production to some extent, with sertraline and aripiprazole consistently and significantly decreasing indole levels. Additional data suggest that this reduction may be, at least in part, driven by observed decreases in key indole-producing taxa, such as *B. ovatus*. In addition to indole, dietary tryptophan can also be metabolised by gut bacteria into indole-3-acetic acid[57] and indole-3-carboxaldehyde[58]. Given that supplementation with these indole derivatives alleviates depression- and anxiety-like behaviours in rodent models[13,55,56], future studies resolving the effects of psychiatric drugs on individual microbiome-derived indole metabolites may provide further insight into their consequences for MGBA signalling.

Both sertraline and aripiprazole influenced SCFA production in microbiomes supplemented with dietary fibre mixes. This effect was particularly pronounced in sertraline-treated microbiomes, where very little microbial translational activity and SCFA production in response to fibre were observed. Reduced SCFA production may have implications for the MGBA, as SCFAs can cross the blood-brain barrier and are present at appreciable concentrations in human cerebrospinal fluid[59,60]. In mice, acetate supplementation ameliorated depressive-like behaviours and restored hippocampal brain-derived neurotrophic factor expression through enhanced histone

acetylation, increased dendritic branching and greater spine density[61]. Similarly, sodium butyrate supplementation reduced depressive symptoms in a lipopolysaccharide-induced mouse model of depression[62]. Together, these findings suggest a potential microbiome-mediated pathway through which sertraline-induced alterations in microbial metabolism could influence host processes relevant to antidepressant responses. Interestingly, a previous study reported that fructooligosaccharide supplementation counteracted sertraline-associated reductions in microbiome functional redundancy and increases in antibiotic resistance proteins[26]. In contrast, our study focused on how psychotropic drugs influence the ability of the gut microbiome to ferment dietary fibres into SCFAs, rather than assessing whether fibre supplementation prior to drug treatment can mitigate drug-induced microbiome perturbations. Contrary to sertraline, aripiprazole increased microbial SCFA production. As elevated colonic SCFA levels have been linked to obesity and enhanced dietary energy harvest[63], this effect could potentially contribute to the weight gain associated with aripiprazole treatment[64]. However, because SCFAs are also implicated in appetite regulation and energy homeostasis[65], further studies are needed to determine whether this relationship is causal.

Not all drugs tested here affected the microbiome to the same extent, and although drug concentration correlated with the magnitude of microbiome perturbation, concentration alone did not explain these differences. For instance, aripiprazole exerted a substantially greater effect than quetiapine, despite its lower estimated colonic concentration, emphasising the value of considering drug structure alongside concentration[23,34]. Here, we identify the dichloro moiety of sertraline as an important determinant of its microbiome toxicity. Sertraline strongly affected membrane-associated functions, including nutrient acquisition, efflux, and energy transduction, whereas the non-chlorinated analogue tametraline had negligible effects. This difference may reflect the greater lipophilicity of sertraline[51], largely conferred by its dichloro moiety[52], which may favour interactions with lipid membranes[66]. Consistent with this, non-antibiotic drugs with greater effects on gut commensals tend to exhibit higher hydrophobicity[23]. Although halogenation and lipophilicity promote SSRI binding within the hydrophobic, halogen-binding pocket of the serotonin transporter protein SERT[67], these same properties may also enhance lipid membrane partitioning and disrupt of microbial membrane function. Similar membrane effects have been reported for other halogenated compounds such as per- and polyfluoroalkyl substances (PFAS), which exhibit toxicity at concentrations comparable to sertraline and alter membrane-associated proteins involved in efflux and nutrient acquisition[45]. Notably, although aripiprazole also contains a dichloro moiety, the position of chlorine substituents can influence physicochemical and biological properties[68], potentially contributing to its distinct effects on the

microbiome. Together, these findings suggest that halogenation and lipophilicity are important determinants of sertraline-induced microbiome toxicity, although the magnitude of this effect may vary across bacterial taxa because of differences in cell-envelope architecture, membrane composition and the capacity to maintain cellular homeostasis under drug-induced stress.

Sertraline also induced pronounced elongation of *B. ovatus* cells. Although elongation can result from stress-induced inhibition of cell division[69], cell division genes were not differentially expressed in sertraline-treated cultures. Instead, the transcriptional downregulation of electron-transfer and redox-associated genes, together with increased membrane permeability, suggests that the membrane-active effect of sertraline compromises cellular energetics, indirectly affecting division. Because bacterial cell division depends on membrane potential for the localisation of cell division proteins[70], sertraline's lipophilicity may facilitate interactions with the cell envelope that interfere with septation and promote elongation. Similar morphological effects have been reported for other amphiphilic psychotropics, with chlorpromazine causing transient filamentation in *E. coli*[71]. These findings support a model in which sertraline, owing to its lipophilicity, partitions into the bacterial membrane, disrupting energy transduction and membrane integrity, with downstream consequences for cell division and growth (Fig. 6d).

While this study advances our understanding of drug-microbiome interactions, it has limitations. Although fresh samples were used to preserve microbial activity in all experiments, which were conducted *ex vivo*, host processes such as drug absorption, distribution, metabolism, and excretion were not captured. Several of the drugs studied may undergo hepatic biotransformation[72,73], and the impact of the resulting drug metabolites on the gut microbiota is unclear. Although the experiments focused on short-term incubations at a single dose of a single drug, the robust effects observed provide a strong foundation for future studies examining chronic exposure *in vivo*. Finally, although the cohort was relatively small, it captured substantial interindividual variation in microbiome responses. Against this heterogenous background, the effects of sertraline were consistently observed across donors, supporting the reproducibility of its impact on the gut microbiome.

Overall, our results suggest that the clinical efficacy and side effects of some, but not all, psychotropic drugs may be compromised by inadvertent drug-microbiome interactions, which alter the availability of key MGBA metabolites, such as indole and SCFAs. One potential approach to counteract this depletion would be to administer probiotics capable of rebalancing levels of these compounds, or via targeted colonic delivery of the metabolites themselves directly[30]. Although the antimicrobial activity of SSRIs such as sertraline has been recognised for

decades[74], the mechanisms behind such effects have remained unclear. Our findings reveal a mechanism whereby sertraline chlorination promotes extensive off-target effects on the gut microbiome. As sertraline and several other halogenated psychotropics are widely used clinically, these findings have broader implications for the prescription of psychotropic drugs.

Materials and Methods

Faecal sample preparation

Faecal sample collection was approved by the Faculty of Environmental and Life Sciences Ethics Committee at the University of Southampton (approval number 78743). All participants signed an informed consent form and questionnaire regarding their mental health status, gastrointestinal health, diet, and exercise habits. Fresh faecal samples were obtained from healthy individuals who had not received antibiotics in the past 3 months and had no diagnosed intestinal disease. They were all provided with a faeces collection kit which included: a Fe-Col faeces catcher (Alpha Laboratories, UK); a universal container with a sampling spoon (Sterilin, UK) and a sealable bag with an Oxoid AnaeroGen sachet (Thermo Scientific Inc.). Each individual self-sampled on the morning of the experiment. The sample was kept anaerobic using an anaerobic sachet (Thermo Fisher) in a sealed bag, until introduction into the anaerobic chamber (Coy Laboratory Products, USA; atmosphere 5% H_2, 10% CO_2 and 85% NO_2). All subsequent sample handling and incubations were performed under anaerobic conditions. The sample was resuspended in 1× phosphate-buffered saline (PBS) to form a 5% w/v faecal slurry and vortexed vigorously for 2-4 min. The faecal slurry was left for 10 min to let large particles settle, and the supernatant was then transferred to a new tube and diluted 1:10 in mGAM medium (HyServe) at 13.9 $g{\cdot}L^{-1}$, to yield a final 0.5% w/v faecal suspension. Remaining large particles were removed by passing the supernatant through a 100 µm cell strainer into a new vial.

Incubation of faecal bacteria with drugs

The 0.5% w/v faecal suspension was diluted to a final concentration of 0.25% w/v in mGAM (13.9 $g{\cdot}L^{-1}$). The drugs were dissolved in dimethyl sulfoxide (DMSO) to create 100× stock solutions and then added to faecal suspensions to achieve final concentrations in the incubations that reflected the estimated concentrations these drugs reach in the colon, based on typical oral doses and their pharmacokinetic profiles[24]: 231 µM sertraline hydrochloride (selective serotonin reuptake inhibitor; Merck, S6319); 113 µM quetiapine hemifumerate (atypical antipsychotic;

Merck, Q3638), 67 µM aripiprazole (atypical antipsychotic; Thermo Scientific Acros, 456170010), 32 µM olanzapine (atypical antipsychotic; MedChemExpress, HY14541) and 1965 µM entacapone (Merck, SML0654). For amitriptyline (tricyclic antidepressant; Merck, A8404) and mirtazapine (tetracyclic antidepressant; Fisher Scientific, 15345058), the colon concentrations are unknown, therefore, an average colon drug concentration of 50 µM was used[22,24]. DMSO was used as a vehicle control, and the final concentration of DMSO in all wells was 1% v/v. Plates were sealed with sterile silicone cap mats (Alpha Laboratories) and incubated at 37 °C, and samples were collected at 0 h (t0), 6 h (t6) and 24 h (t24). At t0, t6 and t24, samples were collected and either preserved in 20% glycerol for cell counts or pelleted, with pellets stored for nucleic acid extraction and supernatants stored for indole quantification. All samples were stored at -80 °C.

Total cell counts by flow cytometry

Flow cytometry was used for the total microbial counts. Samples were diluted as needed in sterile-filtered PBS (0.22 µm) to a final concentration of approximately 1000 cells per µL. Syto9 nucleic acid dye (Invitrogen, Thermo Fisher) was added to the suspension at a final concentration of 0.5 µM, and the suspensions were incubated at room temperature, protected from light, for at least 15 min before running it through a Guava easyCyte cytometer (Merck Millipore), using the 488 nm (Syto9) laser. All sample processing and analyses were performed on the InCyte software (v3.3). Firstly, forward scatter and side scatter thresholds were applied, to remove any debris or noise. Following this, a Syto9- control (an unstained sample) was matched to a Syto9+ sample to establish a gate for microbial cells and exclude background electronic noise or particles. At least 50,000 events were counted for each sample, unless the sample concentration was too low. All samples were processed within 6 h of preparation.

Nucleic acid isolation and 16S rRNA gene amplification and sequencing

Pellets from 500 µL of faecal sample incubations were resuspended in 1 mL InhibitEX Buffer (Qiagen) and transferred to lysis matrix E tubes (MP Biomedicals). Samples were subjected to 3 rounds of bead beating at 40 Hz for 30 s at a time (MP Biomedicals FastPrep-24), with 1 min of cooling on ice in between each treatment. The bead beating tubes were centrifuged at full speed for 10 min before transferring the supernatants into microcentrifuge tubes. Nucleic acid was then extracted according to the manufacturer's protocols (QiAamp Fast DNA Stool Mini Kit) and eluted in nuclease-free water.

Eluted DNA samples were sent to Novogene (Cambridge, UK) for 16S rRNA gene amplicon sequencing. PCR amplification of the 16S V4 region was carried using the primers 515F(5'-GTGCCAGCMGCCGCGGTAA -3')[75] and 806R (5'- GGACTACHVGGGTWTCTAAT -3')[76], followed by library preparation and sequencing on the Illumina NovaSeq 6000 platform to generate paired-end reads of 250 bp.

Preprocessing and analysis of 16S rRNA gene amplicon sequences

Once raw reads were received from Novogene, pre-processing steps were performed using DADA2[77]. FASTQ reads 1 and 2 were first filtered and trimmed at 180 nt and 150 nt, with a maximum expected error threshold of 2 for each read. Forward and reverse reads were merged and chimeric sequences removed. Taxonomy of inferred amplicon sequencing variants (ASVs) was assigned to 16S ribosomal RNA (rRNA) gene/transcript sequences based on SILVA taxonomy (release 138.2) using DADA2. Samples were processed using the vegan (v2.7-5)[78] and phyloseq (v1.54.2)[79] packages of the R software (v4.5.2). The average read count per sample was 59154 ± 8325 high-quality sequences and sample coverage was above 99%. The raw reads per taxon were adjusted according to the copy number of their respective 16S rRNA gene copy, according to rrnDB (v5.8). The ASVs were classified using the RDP classifier on https://rrndb.umms.med.umich.edu/estimate/ prior to the copy number correction. Absolute abundance was obtained by multiplying the corrected abundance by total cell counts[80] determined by flow cytometry. To identify significant differences in ASV abundance, DESeq2 (v1.50.2)[35] was implemented in phyloseq. Only 765 ASVs that had in total ≥10 reads (relative abundance microbial profile) were retained for compositional analyses, and 196 ASVs with greater than 5.0e5 reads (quantitative microbial profile) were considered for comparisons by DESeq2, MaAsLin2 (v1.24.1)[37] and Rhea (v1.2)[81]. All statistical analysis of microbiome data was conducted with the software R (R 4.5.2). The applied significance tests and obtained p-values are referred to in the main text and figure legends.

Metagenomics pipeline

DNA was extracted from drug-incubated samples following the protocol described above, except that triplicate samples from each donor were pooled prior to extraction. Library preparation and shotgun Illumina sequencing were performed by AZENTA on an Illumina NovaSeq 6000 platform to generate paired-end 2x150bp reads at a sequencing depth of ~13 Gb per sample. Paired-end reads were quality filtered and trimmed using fastp (v0.23)[82] using sliding window trimming (window size = 4 bases with mean Phred score >= 20 within each window). Reads shorter than 50

bp after trimming were discarded. Reads were then aligned against the human reference genome (T2T/CHM13, hg39 telomere-to-telomere assembly[83]) and host-derived reads were removed using KneadData (v0.12.4). All outputs were concatenated per sample and run through HUMAnN (v3.9)[36] using MetaPhlAn (4.1.1)[36] with jun23 species-level genome bin markers. HUMAnN outputs were visualised and statistically analysed in the R software using MaAsLin2. MetaPhlAn taxonomic profiles were normalised to microbial counts (averaged per drug per donor) and statistically analysed using MaAsLin2.

Antimicrobial resistance genes (ARGs) were identified from shotgun metagenomic data using the Resistance Gene Identifier (RGI) v6.0.3 and the Comprehensive Antibiotic Resistance Database (CARD)[42]. Quality-filtered reads were aligned to the CARD reference database using the rgi bwt pipeline. To ensure high-confidence identification and minimise false positives, ARGs were filtered at the gene-mapping level. Resistance determinants were considered present only if they met the following criteria: (i) an average breadth of coverage >= 60% of the reference gene length, (ii) an average mapping quality (MAPQ) score >= 10 to ensure reliable assignment to gene families, and (iii) a minimum of 5 mapped reads per Antibiotic Resistance Ontology (ARO) term. To enable quantitative comparison across samples, raw read counts for all filtered ARGs were normalised to Reads Per Kilobase per Million mapped reads (RPKM). This normalisation procedure corrected for potential biases introduced by varying gene lengths and differences in total sequencing depth per sample. Abundance was calculated by dividing the read count of each ARO term by the reference gene length in kilobases, followed by normalisation against the total number of quality-filtered reads for each respective sample.

Indole measurements

Indole concentrations in the supernatant collected from faecal incubations were determined using a colorimetric assay using Kovacs' reagent based on a method previously described[43]. Briefly, supernatants from the incubations were diluted 1:4 in the growth media (mGAM) to a total of 200 µL, in replicates. Subsequently, 200 µL of Kovacs' reagent (Merck) was added. The samples were vortexed and incubated at room temperature for 10 min and subjected to a fast spin (approximately 30 s). The top 100 µL layer was moved to a 96-well plate and absorbance at 530 nm recorded using a plate reader (BMG Labtech POLARstar Omega). Standards (0 µM, 10 µM, 25 µM, 50 µM and 100 µM) of indole (Merck), in triplicates, were prepared in mGAM and processed like the samples to generate a calibration curve. Each day, analysis was quantified using the standard curve made on the same day. We determined the limit of detection to be 10 µM as absorbance readings were inaccurate below this concentration.

Sanger 16S near-full length sequencing

Large colonies were picked from agar plates and resuspended in 50 µL of sterile MilliQ water, before vortexing vigorously for 5-10 s. Next, the tubes were boiled at 95 °C for 10 min to lyse cells, before centrifuging at 14462× *g* for 1 min. Tubes were transferred to ice and supernatant was used for PCR reactions. The DNA was amplified using the primers 27F (5' AGA GTT TGA TCA TGG CTC A-3') and 1492R (5' TAC GGT TAC CTT GTT ACG ACT T-3')[73]. PCR reactions (50 µL) were carried out with 1.25 U of Dream Taq DNA polymerase (Thermo Fisher, UK), 10× Dream Taq buffer (2 mM) (Thermo Fisher, UK), 25 mM $MgCl_2$ (Thermo Fisher, UK), 0.2 mM dNTP mix (Thermo Fisher, UK), 0.2 µM of both forward and reverse primers and 1 to 4 ng of template DNA. The PCR conditions consisted of an initial denaturation at 95 °C for 3 min, followed by 30 cycles of 95 °C for 30 s, annealing at 52 °C for 30 s, and 72 °C for 1 min, followed by a final extension step at 72 °C for 10 min. PCR was carried out in a Bio-Rad T100 thermocycler (Bio-Rad Laboratories). The amplification product was purified using the GeneJET purification kit following manufactures protocol and sequenced by Sanger sequencing (United Kingdom). FASTQ files were obtained and trimmed using SnapGene v7.2.1 and blasted on NCBI.

Fibre mix preparation

Faecal samples were supplemented with two custom-prepared mixes of dietary fibres. Fibre mix 1 (FM1) contained pre-digested (see below) resistant starch from high-amylose corn (Hi-MAIZE 260, Ingredion, Germany), low viscosity arabinoxylan from wheat flour (Megazyme, Ireland) and low viscosity betaglucan from barley (Megazyme, Ireland). Fibre mix 2 (FM2) contained pectin from apple (Merck), inulin from chicory (Merck) and raffinose (D+) pentahydrate (Thermo Fisher). Dietary fibre mixes were supplemented for a final concentration of 1.5% w/v of fibre in incubation samples, with each individual fibre supplemented at a concentration of 0.5% w/v. Resistant starch was pre-digested before incubation to remove any easily digestible components such as amylopectin. This pre-digestion was undertaken since previous studies suggest that the presence of digestible starch components may influence gut microbiome fermentation of indigestible dietary fibres[84]. Briefly, the oral phase of digestion was simulated by adding 60 mL of PBS (pH 6.9) to 5 g of the fibre in a water bath to rehydrate the fibres, before addition of human salivary α-amylase (20 $mg \cdot mL^{-1}$ in 1 M $CaCl_2$) and incubation of the mixture in a shaking water bath at 37 °C for 15 min. After cooling to RT, the gastric phase was initiated by addition of approximately 1.6 mL of 1 M HCl to reduce the pH to 2.5, followed by 2 mL of pepsin (10% w/v in 0.05 M HCl). The mixture was placed on an orbital shaker at 150 rpm at 37 °C for 30 min. The small intestinal phase was then started by adding 10 mL of 0.1 M sodium maleate buffer in 1 mM

$CaCl_2$ and approximately 4 mL $NaHCO_3$ to bring the pH up to 6.9, before immediate addition of 10 mL pancreatin (12.5% w/v in sodium maleate buffer) and 2 mL amyloglucosidase. The mixture was incubated in a shaking water bath at 37 °C for 6 h. Finally, the digested contents were poured into dialysis tubing (molecular weight cut off 12,000-14000 Da; Visking) and dialysed for 3 days against distilled water with changing of water every 12 h. The retentate composed of indigestible starch was frozen at -20 °C overnight and freeze-dried for later use.

Incubation and BONCAT labelling of faecal bacteria with drugs and various carbon sources

The 0.5% w/v faecal suspension was diluted to a final concentration of 0.25% w/v in supplemented M9 mineral medium (sM9)[85], composed of 0.1% L-cysteine, 0.5% v/v of vitamin solution, and 0.1% v/v mineral solution (both prepared according to DSMZ, Medium 461), amended with fibre mix at 1.5% w/v and drugs dissolved in DMSO at a final concentration found in the colon[24], as described earlier. Glucose prepared in sM9 was supplemented to control wells instead of fibre mix (at 0.25% w/v) as it is a simple carbon source and thus, expected to stimulate a significant fraction of the microbial community[34]. The plates were sealed with sterile silicone cap mats (Alpha Laboratories) and incubated at 37 °C for 30 min, before the addition of azidohomoalanine (AHA) (Jena Bioscience, Germany) at a final concentration of 50 µM. At t6, one plate was washed once with 1 mL PBS, before fixing in PBS:ethanol (50% v/v) and storing at -20 °C for click reactions. At t24, 250 µL from all wells were fixed in ethanol for click-chemistry. The remaining sample was separated into pellet and supernatant fractions, and stored at -80 °C.

Click chemistry and microscopy

Fixed samples were vortexed, pelleted, and dehydrated in 96% ethanol for 3 min at room temperature. The dehydrated pellet was resuspended in 221 µL of PBS, and 12.5 µL each of freshly prepared 5 mM sodium ascorbate and 5 mM aminoguanidine hydrochloride were added to the sample and incubated for 3 min. A dye-mix solution was prepared by mixing 100 µM $CuSO_4$, 500 µM THPTA, and 5 µM Sulfo-Cy5-Alkyne dye (Jena Bioscience, Germany). The mixture was incubated for 3 min at room temperature in the dark and then added to the sample. After inversion to mix the dye, the tubes were incubated in the dark at room temperature for 30 min. The cells were then washed twice in 500 µL PBS, and the pellet was finally resuspended in PBS-ethanol (50% v/v).

Upon completion of the click reaction, samples were spotted on to slides, dried, and counterstained with 30 µM 4',6-diamidino-2-phenylindole dihydrochloride (DAPI) in PBS for 15 min before washing with ice-cold water and mounting with CitiFluor AF1 Mounting Medium.

Samples were imaged using an Olympus IX83 inverted fluorescence microscope and a x60 oil objective lens. Images were captured on a Hamamatsu ORCA-Flash4.0 V2 digital CMOS camera, and post-acquisition image editing and analysis was performed using cellSens software (Olympus) and FIJI[86].

Flow cytometry and cell sorting of BONCAT-labelled cells

Flow cytometry was used to determine the fraction of active cells responding to dietary fibres and to sort active, BONCAT+ cells. For activity fractions, samples incubated for 6 h with AHA were first clicked using the protocol described above. Samples were diluted as needed in filtered PBS (0.22 µm) for a final concentration of approximately 1000 cells per µL. Syto9 nucleic acid dye (Invitrogen, Thermo Fisher) was added to the suspension at a final concentration of 0.5 µM, and the suspensions were incubated at room temperature, protected from light, for at least 15 min before running it through a Guava easyCyte cytometer (Merck Millipore), using the 488 nm (Syto9) and 642 nm (Cy5) laser. All sample processing and analyses were performed on the InCyte software. Firstly, forward scatter and side scatter thresholds were applied, to remove any debris or noise. Following this, a Syto9- control was matched to a Syto9+ sample to establish a gate for microbial cells. A Cy5- control was then matched to a Cy5+ sample to establish a Cy5+ (active) gate. Percent active cells were determined by applying a gate for Cy5+ AND Syto9+ counts and dividing by Syto9+ counts. At least 50,000 events were counted for each sample, unless the sample concentration was too low. All samples were processed within 6 h of preparation.

After determining the activity fractions under the different drugs, only the samples which were most significantly different to the control ($P < 0.01$) were selected for sorting on a FACSAria IIu Cell Sorter (Beckton Dickinson). Samples were clicked, stained with Syto9, and sorted within 24 h. At least 100,000 events were sorted for each sample unless concentration was too low. Only events which were both Cy5+ (640 nm red laser) and Syto9+ (488 nm blue laser), using the same sorting strategy as above, were collected. All sorts, as well an aliquot of the PBS, used to dilute the samples, were stored at -80 °C for subsequent DNA extraction.

Nucleic acid isolation and 16S rRNA gene amplicon sequencing of sorted samples

DNA was extracted from sorted fractions using the QIAamp DNA Kit (Qiagen, UK) with an additional enzymatic lysis step. Briefly, sorted fractions were centrifuged at maximum speed for 20 min, and the supernatant was carefully discarded, leaving approximately 100 µL of PBS containing the cell pellet. An enzymatic lysis buffer (200 µL) containing 20 mM Tris-HCl (pH 8.0), 2 mM sodium EDTA, 1.2% Triton X-100, and 20 $mg \cdot mL^{-1}$ lysozyme was added to each sample. All

buffer components, except lysozyme, were UV-irradiated for 30 min prior to use; lysozyme was added immediately before sample processing. Samples were then incubated at 37°C for 30 min, with vortexing every 10 min. Subsequently, 15 µL of proteinase K was added, and the mixture was vortexed. The remaining steps followed the manufacturer's protocol and eluted in nuclease-free water. The PBS aliquot was used as a negative control for sorted samples and processed in parallel with the samples. Fibre mix 1 and fibre mix 2 diluted in M9 to final incubation concentration was also sequenced to identify any contaminants in the dietary fibres.

16S rRNA gene amplification and sequencing of the bacterial DNA were carried out as described above for faecal samples incubated with drugs. The negative PBS control contained a total of 10565 reads, FM1 control contained 70260 reads, and FM2 control contained 62519 reads. The average read count per sample was 57314 ± 12574. Contaminants found in the negative PBS control (ASVs: 234, 344, 389, 403, 406, 452, 458, 482, 490, 516, 533, 562, 583, 616, 663, 703, 714, 807, 961, 971, 1025, 1074 and 1143) and in the fibre mix controls (ASVs: 9, 17, 48, 68, 138, 796, 806 and 836) were removed. ASV_71_Ralstonia_unclassified was also removed from all sorts since it is not typically found within the gut. Although ASVs 1, 91 and 473 were also found in the negative controls, they were not removed as they were present in the samples at a higher abundance, hence we believe that their detection in the controls may be from the well-known low levels of cross-contamination that can be detected when handling multiple samples in parallel. After removing contaminants, copy number correction and pruning any ASVs which had less than 10 reads overall, 313 ASVs were retained. The sample coverage was above 99% for all samples.

SCFA analysis in fibre samples by GC-MS

Short-chain fatty acids (acetic acid, propionic acid, butyric acid, valeric acid) were analysed by gas chromatography – mass spectrometry (GC-MS) using a method adapted from Brignardello et al.[87]. SCFAs were derivatised from the supernatant fractions at t24 of the incubations with the fibre and drug amendments. This process also derivatises SCFAs from the fibre mixes themselves, therefore this background concentration was subtracted from the SCFA concentrations of the incubated samples.

A volume of 100 µL of sample was suspended in 500 µL methyl tert-butyl ether with 2.8 mM 2-ethylbutyric acid as an internal standard (IS) to correct injection variability across the various samples batches and to compensate for analytical drift or minor system instabilities. Subsequently, 0.01% of HCl was added to each sample for acidification and precipitation of

proteins. A short homogenisation step was included by vortexing each tube for 3 s individually, followed by a further 20 min using a plate vortex, after which samples were centrifuged for 5 min at 4 °C at 10,000× *g*. The supernatant was immediately transferred to a silanised vial, and the derivatiser N-tert-butyldimethylsilyl-N-methyltrifluoroacetamide with 1% tert-butyldimethylchloro-silane was added. The sample was incubated for 45 min at 60 °C. Prior to MS analysis, 70 µL of sample was taken into a regular vial with a deactivated insert. GC_MS analysis was performed using an Agilent 6890 Series gas chromatograph (GC) coupled to a 5973 single-quadrupole mass selective detector (MSD) (Agilent Technologies, Palo Alto, CA, USA) along with an Agilent 7683A autosampler. The GC was fitted with an HP-5 MS UI inert capillary column (30-m × 0.25-mm × 0.25-µm film thickness; Agilent J&W Scientific), and helium was used as the carrier gas at 1.0 mL·min^{-1}. Each injection was made in splitless mode with an injection of 1 µL and injector temperature of 260 °C with a solvent delay of 5 min. A glass liner ultra-inert, single-taper and glass wool (5190–2293; Agilent Technologies) was used to avoid possible column contamination with non-volatile elements. The oven temperature program was optimized with an initial temperature of 40 °C and final temperature of 300 °C and the total runtime of the method was 20.53 min. The detection of SCFAs in samples was carried out using full scan mode (m/z 40-400) and the electron impact for the generation of ions was 70eV. The ion source temperature was at 230 °C while the quadrupole temperature was 150 °C. Data were acquired using Agilent ChemStation software on the single quadrupole mass selective detector. The GC-MS assay for SCFAs was validated in terms of linearity using calibration curves for SCFAs standards and accuracy on inter-batch analysis using a QC sample, which was a mixture of 10µl of all the samples tested. The linearity of the standard curves for SCFAs were automatically determined by Agilent ChemStation software. The SCFA standards used were acetic acid (C2), propionic acid (C3), butyric acid (C4), isobutyric acid (i-C4) and valeric acid (C5).

Transcriptomics of *B. ovatus* with sertraline and tametraline amendment

B. ovatus ATCC 8483 (DSM 1896) was selected for transcriptomics with sertraline and tametraline (Molcan Corporation, Canada; Sertraline RC 18). Since sertraline at 231 µM completely inhibited growth of *B. ovatus*, a minimum inhibitory concentration (MIC) assay was performed to determine a concentration of sertraline which would still exert pressure on the bacteria without complete inhibition (25 µM). Thereafter, a growth curve of *B. ovatus* grown in mGAM 1:3 with 1 µg·mL^{-1} vitamin K1 and 5 µg·mL^{-1} hemin amended with 1% DMSO, 25 µM sertraline and 25 µM tametraline was assessed to find a mid-exponential OD_{600} at which cultures could be collected for RNA extraction. *B. ovatus* was first streaked from a glycerol stock on to an

mGAM 1:3 agar plate and grown anaerobically for 36 h. Individual colonies were inoculated in mGAM 1:3 supplemented with vitamin K1 and hemin and grown to turbid cultures overnight. These cultures were then inoculated 1:100 in 6.5 mL fresh media and amended with the various drug treatments above in triplicate. When cultures reached mid-exponential phase (~0.55 OD_{600}), they were removed from the anaerobic chamber and immediately fixed with 650 µL (1:10 v/v) of an ice-cold mixture of acid-phenol and ethanol (2.5 mL water equilibrated phenol (Severn Biotech Ltd.) and 47.5 mL ethanol). Samples were vortexed gently, followed by 5 min incubation on ice. All samples were transferred to 15 mL tubes and centrifuged at 4000 g for 5 min. Supernatant was discarded and pellets were stored at -80 °C. *B. ovatus* culture pellets were defrosted on ice, homogenised in 100 µL of TE-Lysozyme buffer, and incubated at 37°C for 15 min. Total RNA was isolated from pellets using the Total RNA Purification Kit (Norgen Biotek #17200) according to manufacturer's protocols. Crude nucleic acid extract (41 µL) DNase treatment (TURBO DNAse 2 $U \cdot \mu L^{-1}$, Thermo Fischer Scientific) carried out according to the manufacturer's instructions. Samples were incubated at 37 °C with gentle shaking (250 rpm) for 30 min, after which an additional 1 µL of DNase was added to each tube, and the incubation step was repeated (30 min, 37 °C, 250 rpm). Following DNase treatment, the Zymo RNA Clean & Concentrator Kit (Zymo Research) was used to clean and purify the final RNA according to manufacturer's instructions. Purified total RNA was sent to AZENTA for quality control, library construction, sequencing, and analysis. Briefly, ribosomal RNA was depleted from total RNA, followed by RNA fragmentation and random priming. First- and second-strand cDNA synthesis was then performed. The resulting double-stranded cDNA underwent end repair, 5' phosphorylation, and dA-tailing. Finally, adapter ligation, PCR enrichment, and sequencing of the multiplexed libraries were carried out on an Illumina NovaSeq 6000 platform. Sequencing yielded an average of 16.9 ± 4.7 M reads per sample. Following sequencing, raw reads were demultiplexed, low-quality bases and adapter sequences were trimmed, and high-quality clean reads were retained for downstream alignment to the provided *B. ovatus* ATCC 8483 reference genome (GCF_001314995.1, assembly ASM131499v1), and differential expression analysis with DESeq2.

Scanning electron microscopy of *B. ovatus*

B. ovatus cultures were supplemented with 30 µM of sertraline and 30 µM of tametraline (both drugs dissolved in DMSO), or DMSO alone as a control, and cultured as described above. Samples were collected at the exponential growth phase, centrifuged at 5000× *g* for 5 min at RT, and fixed by resuspending the pellet in 2.5% glutaraldehyde in 0.1 M cacodylate buffer (pH 7.2)

for 1 h at RT. Fixed cells were stored at 4 °C until further processing. 100 µl of fixed cell suspension was applied to aminopropyltriethoxysilane (APES)-coated glass coverslips for 30 min in a humid chamber. To prepare APES-coated glass coverslips, 13x13 mm glass coverslips were cleaned in 1% acid alcohol (1% v/v HCl, 70% ethanol) for 30 min, rinsed in water, air-dried, dehydrated in acetone for 10 min, and coated with 2% (v/v) APES in acetone for 5 min, then rinsed twice in distilled water before drying and storage. Coated coverslips containing the fixed cell suspension were washed twice in cacodylate buffer for 5 min each, and then post-fixed in 1% osmium tetroxide in 0.1 M cacodylate buffer for 30 min, washed in deionised water, and dehydrated through a graded ethanol series (30–100%, 10 min per step). Samples were critical-point dried using a Balzers CPD 030 critical point drier, mounted onto aluminium stubs, and sputter-coated with 7nm of platinum (Quorum Q150T) prior to imaging. Samples were imaged (immersion mode with T2 detector; ThermoFisher Apreo 2 SEM) at an accelerating voltage of 10 kV, with working distance and magnification adjusted as needed per image.

Propidium iodide staining of *B. ovatus*

Bacterial cultures were supplemented with drugs and grown anaerobically as described above. Samples were collected at the exponential growth phase, centrifuged at 5000× *g* for 5 min at RT and resuspended in PBS. Syto9 nucleic acid dye (Invitrogen, Thermo Fisher) and propidium iodide (Merck) were added to the cultures to final concentrations of 0.83 µM and 9.9 µM, respectively. Samples were incubated for 15 min at room temperature in the dark, in an anaerobic chamber. Following staining, cells were centrifuged and resuspended gently in PBS. Samples were removed from the anaerobic chamber and immediately fixed by adding 1 vol. of 4% paraformaldehyde in PBS. After fixation for 1 h at room temperature, cells were washed once with PBS and finally resuspended in PBS. Finally, 10 µL of the cell suspension was applied onto a glass slide and mounted using CitiFluor AF1 Mounting Medium. Samples were imaged using an Olympus IX83 inverted fluorescence microscope and a x100 oil objective lens. Images were captured on a Hamamatsu ORCA-Flash4.0 V2 digital CMOS camera, and post-acquisition image editing and analysis was performed using cellSens software (Olympus) and FIJI[86].

Statistical analysis and visualisation

All statistical analyses and visualisation were performed in R (v4.5.2) with the ggpubr package[88], rstatix package and the ggplot2 package[89]. *P*-values and statistical tests are indicated in figures and figure legends. $P < 0.05$ was considered statistically significant across all conducted experiments.

Data Availability Statement

The 16S rRNA gene sequences were deposited in the NCBI (www.ncbi.nlm.nih.gov) Sequence Read Archive (SRA) under project number PRJNA1515986. Shotgun metagenomic and RNA-Seq data are also available at NCBI under the same project (PRJNA1515986).

Acknowledgements

We would like to thank Carolann MacGuire and Sarah Pearson from the Faculty of Medicine Flow Cytometry Core Facility, University of Southampton for their assistance with flow cytometry. We also thank Mark Willett and the Imaging, Microscopy & Cytometry Centre, University of Southampton. Finally, we thank Regan Doherty at the Biomedical Imaging Unit, University of Southampton for her assistance with scanning electron microscopy.

References

1 Valles-Colomer, M. *et al*. The neuroactive potential of the human gut microbiota in quality of life and depression. *Nat Microbiol* **4**, 623-632 (2019). https://doi.org/10.1038/s41564-018-0337-x

2 Bercik, P. *et al*. The anxiolytic effect of Bifidobacterium longum NCC3001 involves vagal pathways for gut–brain communication. *Neurogastroenterol. Motil.* **23**, 1132-1139 (2011). https://doi.org/https://doi.org/10.1111/j.1365-2982.2011.01796.x

3 Miyaoka, T. *et al*. Clostridium butyricum MIYAIRI 588 as Adjunctive Therapy for Treatment-Resistant Major Depressive Disorder: A Prospective Open-Label Trial. *Clin. Neuropharmacol.* **41**, 151-155 (2018). https://doi.org/10.1097/wnf.0000000000000299

4 Cryan, J. F. *et al*. The Microbiota-Gut-Brain Axis. *Physiol. Rev.* **99**, 1877-2013 (2019). https://doi.org/10.1152/physrev.00018.2018

5 Yano, Jessica M. *et al*. Indigenous Bacteria from the Gut Microbiota Regulate Host Serotonin Biosynthesis. *Cell* **161**, 264-276 (2015). https://doi.org/10.1016/j.cell.2015.02.047

6 McVey Neufeld, K.-A. *et al*. Oral selective serotonin reuptake inhibitors activate vagus nerve dependent gut-brain signalling. *Sci. Rep.* **9**, 14290 (2019). https://doi.org/10.1038/s41598-019-50807-8

7 Onimus, O. *et al*. The gut-brain vagal axis governs mesolimbic dopamine dynamics and reward events. *Science Advances* **12**, eadz0828 (2026). https://doi.org/doi:10.1126/sciadv.adz0828

8 Sasso, J. M. *et al*. Gut Microbiome–Brain Alliance: A Landscape View into Mental and Gastrointestinal Health and Disorders. *ACS Chem. Neurosci.* **14**, 1717-1763 (2023). https://doi.org/10.1021/acschemneuro.3c00127

9 Bravo, J. A. *et al.* Ingestion of Lactobacillus strain regulates emotional behavior and central GABA receptor expression in a mouse via the vagus nerve. *PNAS* **108**, 16050-16055 (2011). https://doi.org/doi:10.1073/pnas.1102999108

10 Frost, G. *et al.* The short-chain fatty acid acetate reduces appetite via a central homeostatic mechanism. *Nat Commun* **5**, 3611 (2014). https://doi.org/10.1038/ncomms4611

11 Berding, K. *et al.* Feed your microbes to deal with stress: a psychobiotic diet impacts microbial stability and perceived stress in a healthy adult population. *Mol. Psychiatry* **28**, 601-610 (2023). https://doi.org/10.1038/s41380-022-01817-y

12 Delgado, I. *et al.* Association between the indole pathway of tryptophan metabolism and subclinical depressive symptoms in obesity: a preliminary study. *Int. J. Obes.* **46**, 885-888 (2022). https://doi.org/10.1038/s41366-021-01049-0

13 Chen, Y. *et al.* Indole Acetic Acid Exerts Anti-Depressive Effects on an Animal Model of Chronic Mild Stress. *Nutrients* **14** (2022). https://doi.org/10.3390/nu14235019

14 Shoaie, S. *et al.* Understanding the interactions between bacteria in the human gut through metabolic modeling. *Sci. Rep.* **3**, 2532 (2013). https://doi.org/10.1038/srep02532

15 Desai, M. S. *et al.* A Dietary Fiber-Deprived Gut Microbiota Degrades the Colonic Mucus Barrier and Enhances Pathogen Susceptibility. *Cell* **167**, 1339-1353.e1321 (2016). https://doi.org/https://doi.org/10.1016/j.cell.2016.10.043

16 Soret, R. *et al.* Short-Chain Fatty Acids Regulate the Enteric Neurons and Control Gastrointestinal Motility in Rats. *Gastroenterology* **138**, 1772-1782.e1774 (2010). https://doi.org/https://doi.org/10.1053/j.gastro.2010.01.053

17 Schiweck, C. *et al.* Circulating Short Chain Fatty Acids are Associated with Depression Severity and Predict Remission from Major Depressive Disorder. *Brain, Behavior, & Immunity - Health*, 101070 (2025). https://doi.org/https://doi.org/10.1016/j.bbih.2025.101070

18 Dalile, B., Van Oudenhove, L., Vervliet, B. & Verbeke, K. The role of short-chain fatty acids in microbiota–gut–brain communication. *Nature Reviews Gastroenterology & Hepatology* **16**, 461-478 (2019). https://doi.org/10.1038/s41575-019-0157-3

19 Ait Chait, Y., Mottawea, W., Tompkins, T. A. & Hammami, R. Evidence of the Dysbiotic Effect of Psychotropics on Gut Microbiota and Capacity of Probiotics to Alleviate Related Dysbiosis in a Model of the Human Colon. *Int. J. Mol. Sci.* **24** (2023). https://doi.org/10.3390/ijms24087326

20 Zimmermann, M., Patil, K. R., Typas, A. & Maier, L. Towards a mechanistic understanding of reciprocal drug–microbiome interactions. *Mol. Syst. Biol.* **17** (2021). https://doi.org/10.15252/msb.202010116

21 Garcia-Santamarina, S. *et al.* Emergence of community behaviors in the gut microbiota upon drug treatment. *Cell* **187**, 6346-6357.e6320 (2024). https://doi.org/https://doi.org/10.1016/j.cell.2024.08.037

22 Klünemann, M. *et al.* Bioaccumulation of therapeutic drugs by human gut bacteria. *Nature* **597**, 533-538 (2021). https://doi.org/10.1038/s41586-021-03891-8

23 Grießhammer, A. *et al.* Non-antibiotics disrupt colonization resistance against enteropathogens. *Nature* **644**, 497-505 (2025). https://doi.org/10.1038/s41586-025-09217-2

24 Maier, L. *et al.* Extensive impact of non-antibiotic drugs on human gut bacteria. *Nature* **555**, 623-628 (2018). https://doi.org/10.1038/nature25979

25 Aasmets, O., Taba, N., Krigul, K. L., Andreson, R. & Org, E. A hidden confounder for microbiome studies: medications used years before sample collection. *mSystems* **0**, e00541-00525 https://doi.org/doi:10.1128/msystems.00541-25

26 Li, L. *et al.* Systematic metaproteomics mapping reveals functional and ecological landscapes of Ex vivo human gut microbiota responses to therapeutic drugs. *Nature Communications* **16**, 9383 (2025). https://doi.org/10.1038/s41467-025-64433-8

27 Doll, J. P. K. *et al.* Fecal Microbiota Transplantation (FMT) as an Adjunctive Therapy for Depression—Case Report. *Front Psychiatry* **13** (2022). https://doi.org/10.3389/fpsyt.2022.815422

28 Kalow, W., Tang, B. K. & Endrenyi, L. Hypothesis: comparisons of inter- and intra-individual variations can substitute for twin studies in drug research. *Pharmacogenetics* **8**, 283-289 (1998). https://doi.org/10.1097/00008571-199808000-00001

29 Saad, R., Rizkallah, M. R. & Aziz, R. K. Gut Pharmacomicrobiomics: the tip of an iceberg of complex interactions between drugs and gut-associated microbes. *Gut Pathog.* **4**, 16 (2012). https://doi.org/10.1186/1757-4749-4-16

30 de la Cuesta-Zuluaga, J., Müller, P. & Maier, L. Balancing act: counteracting adverse drug effects on the microbiome. *Trends Microbiol.* **33**, 268-276 (2025). https://doi.org/10.1016/j.tim.2024.09.011

31 Gray, K. *Medicines Used in Mental Health – England – 2015/16 to 2021/22*, <https://www.nhsbsa.nhs.uk/statistical-collections/medicines-used-mental-health-england/medicines-used-mental-health-england-201516-202122> (2022).

32 Cummings, J. H., Pomare, E. W., Branch, W. J., Naylor, C. P. & Macfarlane, G. T. Short chain fatty acids in human large intestine, portal, hepatic and venous blood. *Gut* **28**, 1221-1227 (1987). https://doi.org/10.1136/gut.28.10.1221

33 Candeliere, F. *et al.* Indole and p-cresol in feces of healthy subjects: Concentration, kinetics, and correlation with microbiome. *Front Mol Med* **2**, 959189 (2022). https://doi.org/10.3389/fmmed.2022.959189

34 Pereira, F. C. *et al.* The Parkinson's disease drug entacapone disrupts gut microbiome homeostasis via iron sequestration. *Nat Microbiol* **9**, 3165-3183 (2024). https://doi.org/10.1038/s41564-024-01853-0

35 Love, M. I., Huber, W. & Anders, S. Moderated estimation of fold change and dispersion for RNA-seq data with DESeq2. *Genome Biol.* **15**, 550 (2014). https://doi.org/10.1186/s13059-014-0550-8

36 Beghini, F. *et al.* Integrating taxonomic, functional, and strain-level profiling of diverse microbial communities with bioBakery 3. *eLife* **10**, e65088 (2021). https://doi.org/10.7554/eLife.65088

37 Mallick, H. *et al*. Multivariable association discovery in population-scale meta-omics studies. *PLOS Computational Biology* **17**, e1009442 (2021). https://doi.org/10.1371/journal.pcbi.1009442

38 Caspi, R. *et al*. The MetaCyc database of metabolic pathways and enzymes and the BioCyc collection of Pathway/Genome Databases. *Nucleic Acids Res*. **42**, D459-D471 (2014). https://doi.org/10.1093/nar/gkt1103

39 Hillege Lars, E. *et al*. Microbial vitamin biosynthesis links gut microbiota dynamics to chemotherapy toxicity. *mBio* **16**, e00930-00925 (2025). https://doi.org/10.1128/mbio.00930-25

40 Kim, H.-B., Cho, Y.-J. & Choi, S. S. Metformin increases gut multidrug resistance genes in type 2 diabetes, potentially linked to Escherichia coli. *Sci. Rep*. **14**, 21480 (2024). https://doi.org/10.1038/s41598-024-72467-z

41 Kyono, Y., Magboo, J. D., Daley, E. A. & Flowers, S. A. Antipsychotic quetiapine alters the mouse fecal resistome by impacting antibiotic efflux, cell membrane, and cell wall synthesis genes. *Microbiology Spectrum* **12**, e03804-03823 (2024). https://doi.org/doi:10.1128/spectrum.03804-23

42 Alcock, B. P. *et al*. CARD 2023: expanded curation, support for machine learning, and resistome prediction at the Comprehensive Antibiotic Resistance Database. *Nucleic Acids Res*. **51**, D690-d699 (2023). https://doi.org/10.1093/nar/gkac920

43 Sinha, A. K. *et al*. Dietary fibre directs microbial tryptophan metabolism via metabolic interactions in the gut microbiota. *Nat Microbiol* **9**, 1964-1978 (2024). https://doi.org/10.1038/s41564-024-01737-3

44 Hatzenpichler, R. *et al*. *In situ* visualization of newly synthesized proteins in environmental microbes using amino acid tagging and click chemistry. *Environ. Microbiol*. **16**, 2568-2590 (2014). https://doi.org/10.1111/1462-2920.12436

45 Lindell, A. E. *et al*. Human gut bacteria bioaccumulate per- and polyfluoroalkyl substances. *Nature Microbiology* **10**, 1630-1647 (2025). https://doi.org/10.1038/s41564-025-02032-5

46 Koe, B. K., Weissman, A., Welch, W. M. & Browne, R. G. Sertraline, 1S,4S-N-methyl-4-(3,4-dichlorophenyl)-1,2,3,4-tetrahydro-1-naphthylamine, a new uptake inhibitor with selectivity for serotonin. *The Journal of Pharmacology and Experimental Therapeutics* **226**, 686-700 (1983). https://doi.org/https://doi.org/10.1016/S0022-3565(25)21773-6

47 Redder, P., Hausmann, S., Khemici, V., Yasrebi, H. & Linder, P. Bacterial versatility requires DEAD-box RNA helicases. *FEMS Microbiol. Rev*. **39**, 392-412 (2015). https://doi.org/10.1093/femsre/fuv011

48 Graumann, P. L. & Marahiel, M. A. A superfamily of proteins that contain the cold-shock domain. *Trends Biochem. Sci*. **23**, 286-290 (1998). https://doi.org/https://doi.org/10.1016/S0968-0004(98)01255-9

49 Yu, N. Y. *et al*. PSORTb 3.0: improved protein subcellular localization prediction with refined localization subcategories and predictive capabilities for all prokaryotes. *Bioinformatics* **26**, 1608-1615 (2010). https://doi.org/10.1093/bioinformatics/btq249

50 Kaoutari, A. E., Armougom, F., Gordon, J. I., Raoult, D. & Henrissat, B. The abundance and variety of carbohydrate-active enzymes in the human gut microbiota. *Nature Reviews Microbiology* **11**, 497-504 (2013). https://doi.org/10.1038/nrmicro3050

51 Kim, S. *et al*. PubChem 2025 update. *Nucleic Acids Res*. **53**, D1516-D1525 (2025). https://doi.org/10.1093/nar/gkae1059

52 Joshi, S. & Srivastava, R. Effect of “magic chlorine” in drug discovery: an in silico approach. *RSC Advances* **13**, 34922-34934 (2023). https://doi.org/10.1039/d3ra06638j

53 (!!! INVALID CITATION !!! 27,53).

54 Tarkesh, F., Namavar Jahromi, B., Hejazi, N. & Hoseini, G. Effect of vitamin K2 administration on depression status in patients with polycystic ovary syndrome: a randomized clinical trial. *BMC Womens Health* **22**, 315 (2022). https://doi.org/10.1186/s12905-022-01825-8

55 Wang, X., Liu, R., Liu, J., Lin, Y. & Zhou, M. Gut microbiota-derived indole metabolites in depression: mechanisms and therapeutic potential. *Eur. J. Pharmacol*. **1019**, 178720 (2026). https://doi.org/https://doi.org/10.1016/j.ejphar.2026.178720

56 Wei, G. Z. *et al*. Tryptophan-metabolizing gut microbes regulate adult neurogenesis via the aryl hydrocarbon receptor. *PNAS* **118**, e2021091118 (2021). https://doi.org/doi:10.1073/pnas.2021091118

57 Li, H. *et al*. Gut microbiota-derived indole-3-acetic acid suppresses high myopia progression by promoting type I collagen synthesis. *Cell Discovery* **10**, 89 (2024). https://doi.org/10.1038/s41421-024-00709-5

58 Huang, Y.-X. *et al*. Gut microbiome-derived indole-3-carboxaldehyde promotes intestinal development via AHR-NRF2 signaling in the early-life of chicks. *Microbiome* **14**, 34 (2025). https://doi.org/10.1186/s40168-025-02289-2

59 Fillier, T. A. *et al*. Brief exposure of neuronal cells to levels of SCFAs observed in human systemic circulation impair lipid metabolism resulting in apoptosis. *Sci. Rep*. **12**, 14355 (2022). https://doi.org/10.1038/s41598-022-18363-w

60 Wishart, D. S. *et al*. HMDB 4.0: the human metabolome database for 2018. *Nucleic Acids Res*. **46**, D608-D617 (2018). https://doi.org/10.1093/nar/gkx1089

61 Huang, W. *et al*. Acetate supplementation produces antidepressant-like effect via enhanced histone acetylation. *J. Affect. Disord*. **281**, 51-60 (2021). https://doi.org/10.1016/j.jad.2020.11.121

62 Qiu, J. *et al*. Lipopolysaccharide-induced depression-like behaviors is ameliorated by sodium butyrate via inhibiting neuroinflammation and oxido-nitrosative stress. *Pharmacology* **105**, 550-560 (2020).

63 Rahat-Rozenbloom, S., Fernandes, J., Gloor, G. B. & Wolever, T. M. S. Evidence for greater production of colonic short-chain fatty acids in overweight than lean humans. *International Journal of Obesity* **38**, 1525-1531 (2014). https://doi.org/10.1038/ijo.2014.46

64 Wu, H. *et al*. Antipsychotic-Induced Weight Gain: Dose-Response Meta-Analysis of Randomized Controlled Trials. *Schizophr. Bull.* **48**, 643-654 (2022). https://doi.org/10.1093/schbul/sbac001

65 Byrne, C. S., Chambers, E. S., Morrison, D. J. & Frost, G. The role of short chain fatty acids in appetite regulation and energy homeostasis. *Int. J. Obes.* **39**, 1331-1338 (2015). https://doi.org/10.1038/ijo.2015.84

66 Wang, Z., Felstead, H. R., Troup, R. I., Linclau, B. & Williamson, P. T. F. Lipophilicity Modulations by Fluorination Correlate with Membrane Partitioning. *Angewandte Chemie International Edition* **62**, e202301077 (2023). https://doi.org/https://doi.org/10.1002/anie.202301077

67 Zhou, Z. *et al*. Antidepressant specificity of serotonin transporter suggested by three LeuT–SSRI structures. *Nat. Struct. Mol. Biol.* **16**, 652-657 (2009). https://doi.org/10.1038/nsmb.1602

68 Staroń, J. *et al*. Tuning the activity of known drugs via the introduction of halogen atoms, a case study of SERT ligands – Fluoxetine and fluvoxamine. *Eur. J. Med. Chem.* **220**, 113533 (2021). https://doi.org/https://doi.org/10.1016/j.ejmech.2021.113533

69 Tran, T. D., Ali, M. A., Lee, D., Félix, M.-A. & Luallen, R. J. Bacterial filamentation as a mechanism for cell-to-cell spread within an animal host. *Nature Communications* **13**, 693 (2022). https://doi.org/10.1038/s41467-022-28297-6

70 Strahl, H. & Hamoen, L. W. Membrane potential is important for bacterial cell division. *Proceedings of the National Academy of Sciences* **107**, 12281-12286 (2010). https://doi.org/doi:10.1073/pnas.1005485107

71 Amaral, L. & Lorian, V. Effects of chlorpromazine on the cell envelope proteins of Escherichia coli. *Antimicrob. Agents Chemother.* **35**, 1923-1924 (1991). https://doi.org/doi:10.1128/aac.35.9.1923

72 Cooper, J. M., Duffull, S. B., Saiao, A. S. & Isbister, G. K. The pharmacokinetics of sertraline in overdose and the effect of activated charcoal. *Br. J. Clin. Pharmacol.* **79**, 307-315 (2015). https://doi.org/10.1111/bcp.12500

73 Kneller, L. A., Zubiaur, P., Koller, D., Abad-Santos, F. & Hempel, G. Influence of CYP2D6 Phenotypes on the Pharmacokinetics of Aripiprazole and Dehydro-Aripiprazole Using a Physiologically Based Pharmacokinetic Approach. *Clin. Pharmacokinet.* **60**, 1569-1582 (2021). https://doi.org/10.1007/s40262-021-01041-x

74 Munoz-Bellido, J. L., Munoz-Criado, S. & Garcìa-Rodrìguez, J. A. Antimicrobial activity of psychotropic drugs: Selective serotonin reuptake inhibitors. *Int. J. Antimicrob. Agents* **14**, 177-180 (2000). https://doi.org/https://doi.org/10.1016/S0924-8579(99)00154-5

75 Parada, A. E., Needham, D. M. & Fuhrman, J. A. Every base matters: assessing small subunit rRNA primers for marine microbiomes with mock communities, time series and global field samples. *Environ. Microbiol.* **18**, 1403-1414 (2016). https://doi.org/10.1111/1462-2920.13023

76 Apprill, A., McNally, S., Parsons, R. & Weber, L. Minor revision to V4 region SSU rRNA 806R gene primer greatly increases detection of SAR11 bacterioplankton. *Aquat. Microb. Ecol.* **75**, 129-137 (2015).

77 Callahan, B. J. *et al.* DADA2: High-resolution sample inference from Illumina amplicon data. *Nat. Methods* **13**, 581-583 (2016). https://doi.org/10.1038/nmeth.3869

78 Oksanen, J. *et al.* (2023).

79 McMurdie, P. J. & Holmes, S. phyloseq: An R Package for Reproducible Interactive Analysis and Graphics of Microbiome Census Data. *PLoS One* **8**, e61217 (2013). https://doi.org/10.1371/journal.pone.0061217

80 Vandeputte, D. *et al.* Quantitative microbiome profiling links gut community variation to microbial load. *Nature* **551**, 507-511 (2017). https://doi.org/10.1038/nature24460

81 Lagkouvardos, I., Fischer, S., Kumar, N. & Clavel, T. Rhea: a transparent and modular R pipeline for microbial profiling based on 16S rRNA gene amplicons. *PeerJ* **5**, e2836 (2017). https://doi.org/10.7717/peerj.2836

82 Chen, S. fastp 1.0: An ultra-fast all-round tool for FASTQ data quality control and preprocessing. *iMeta* **4**, e70078 (2025). https://doi.org/https://doi.org/10.1002/imt2.70078

83 Nurk, S. *et al.* The complete sequence of a human genome. *Science* **376**, 44-53 (2022). https://doi.org/doi:10.1126/science.abj6987

84 Klostermann, C. E. *et al.* Presence of digestible starch impacts in vitro fermentation of resistant starch. *Food Funct.* **15**, 223-235 (2024). https://doi.org/10.1039/D3FO01763J

85 Flanagan, K. *et al.* Human-derived microRNA 21 regulates indole and L-tryptophan biosynthesis transcripts in the gut commensal Bacteroides thetaiotaomicron. *mBio* **16**, e03928-03924 (2025). https://doi.org/doi:10.1128/mbio.03928-24

86 Schindelin, J. *et al.* Fiji: an open-source platform for biological-image analysis. *Nat. Methods* **9**, 676-682 (2012). https://doi.org/10.1038/nmeth.2019

87 Brignardello, J. *et al.* Characterization of diet-dependent temporal changes in circulating short-chain fatty acid concentrations: A randomized crossover dietary trial. *The American Journal of Clinical Nutrition* **116**, 1368-1378 (2022).

88 Kassambara, A. *ggpubr: 'ggplot2' Based Publication Ready Plots*, <https://rpkgs.datanovia.com/ggpubr/> (2023).

89 Wickham, H. *ggplot2: Elegant Graphics for Data Analysis*. (Springer-Verlag New York, 2016).

Supplementary Files

This is a list of supplementary files associated with this preprint. Click to download.

- Shazzadetalsupplementary271026final.pdf
- SupplementaryTablesManuscript271026final.xlsx